Targeted macrophage phagocytosis by Irg1/itaconate axis improves the prognosis of intracerebral hemorrhagic stroke and peritonitis

Zhaoli Luo,[a] Ziyang Sheng,[b] Liye Hu,[a] Lei Shi,[a] Yichen Tian,[c] Xiaochu Zhao,[c] Wei Yang,[b] Zhongnan Xiao,[a] Danmin Shen,[a] Weihua Wu,[a] Ting Lan,[a] Boqian Zhao,[c] Xiaogang Wang,[c] Nan Zhuang,[a] Jian-Nan Zhang,[d] Yamei Wang,[a] Yabin Lu,[a] Liyong Wang,[e] Chenguang Zhang,[a] Peipei Wang,[d] Jing An,[b] Fei Yang,[d,f,**] and Qian Li[a,f,g,*]

[a]Department of Biochemistry and Molecular Biology, School of Basic Medical Sciences, Capital Medical University, Beijing 100069, China
[b]Department of Microbiology, School of Basic Medical Sciences, Capital Medical University, Beijing 100069, China
[c]School of Basic Medical Sciences, Capital Medical University, Beijing 100069, China
[d]Department of Neurobiology, School of Basic Medical Sciences, Capital Medical University, Beijing 100069, China
[e]Core Facilities for Molecular Biology, Capital Medical University, Beijing 100069, China
[f]Laboratory for Clinical Medicine, Beijing Key Laboratory of Neural Regeneration and Repair, Capital Medical University, Beijing 100069, China
[g]Beijing Key Laboratory of Cancer Invasion and Metastasis Research, Capital Medical University, Beijing 100069, China

eBioMedicine
2024;101: 104993
Published Online xxx
https://doi.org/10.1016/j.ebiom.2024.104993

Summary

Background Macrophages are innate immune cells whose phagocytosis function is critical to the prognosis of stroke and peritonitis. *cis*-aconitic decarboxylase immune-responsive gene 1 (Irg1) and its metabolic product itaconate inhibit bacterial infection, intracellular viral replication, and inflammation in macrophages. Here we explore whether itaconate regulates phagocytosis.

Methods Phagocytosis of macrophages was investigated by time-lapse video recording, flow cytometry, and immunofluorescence staining in macrophage/microglia cultures isolated from mouse tissue. Unbiased RNA-sequencing and ChIP-sequencing assays were used to explore the underlying mechanisms. The effects of Irg1/itaconate axis on the prognosis of intracerebral hemorrhagic stroke (ICH) and peritonitis was observed in transgenic (*Irg1*$^{flox/flox}$; *Cx3cr1*$^{creERT/+}$, cKO) mice or control mice *in vivo*.

Findings In a mouse model of ICH, depletion of *Irg1* in macrophage/microglia decreased its phagocytosis of erythrocytes, thereby exacerbating outcomes (n = 10 animals/group, $p < 0.05$). Administration of sodium itaconate/4-octyl itaconate (4-OI) promoted macrophage phagocytosis (n = 7 animals/group, $p < 0.05$). In addition, in a mouse model of peritonitis, *Irg1* deficiency in macrophages also inhibited phagocytosis of *Staphylococcus aureus* (n = 5 animals/group, $p < 0.05$) and aggravated outcomes (n = 9 animals/group, $p < 0.05$). Mechanistically, 4-OI alkylated cysteine 155 on the Kelch-like ECH-associated protein 1 (Keap1), consequent in nuclear translocation of nuclear factor erythroid 2-related factor 2 (Nrf2) and transcriptional activation of *Cd36* gene. Blocking the function of CD36 completely abolished the phagocytosis-promoting effects of Irg1/itaconate axis *in vitro* and *in vivo*.

Interpretation Our findings provide a potential therapeutic target for phagocytosis-deficiency disorders, supporting further development towards clinical application for the benefit of stroke and peritonitis patients.

Funding The National Natural Science Foundation of China (32070735, 82371321 to Q. Li, 82271240 to F. Yang) and the Beijing Natural Science Foundation Program and Scientific Research Key Program of Beijing Municipal Commission of Education (KZ202010025033 to Q. Li).

Keywords: Irg1; Itaconate; Macrophage; Phagocytosis; Intracerebral hemorrhagic stroke; Peritonitis

*Corresponding author.
**Corresponding author.
E-mail addresses: qianli@ccmu.edu.cn (Q. Li), feiyang@ccmu.edu.cn (F. Yang).

Research in context

Evidence before this study

Phagocytosis inefficiency/dysfunction of macrophages is closely related to the occurrence or worsening of various diseases. Literatures have shown that the size of the hematoma after ICH is a well-established predictor of clinical outcomes in patients, and that the decreased phagocytosis and bactericidal ability of host peritoneal macrophages may contribute to bacterial peritonitis. With a focus on phagocytosis, enhanced antibody-dependent macrophage phagocytosis has been successfully used as a cancer immunotherapy in the clinic. Nevertheless, how to enhance macrophage phagocytosis in other diseases requires further research and clinical translation.

Added value of this study

In this work, we demonstrated that Irg1/itaconate axis significantly promoted phagocytosis in macrophages and improved prognosis in mouse models of ICH and acute peritonitis. Mechanistically, with unbiased RNA-sequencing and ChIP-sequencing assays, we uncovered that itaconate alkylated the Kelch-like ECH-associated protein 1 (Keap1), consequently increased the nuclear translocation of nuclear factor erythroid 2-related factor 2 (Nrf2), and subsequently increased the expression of scavenger receptor coding gene *Cd36*.

Implications of all the available evidence

Our work is the first to demonstrate the novel role of Irg1/itaconate axis in the promotion of phagocytosis in different sources of macrophages (mouse bone marrow-derived macrophages, primary microglia, and peritoneal macrophages), and uncover the Irg1/itaconate axis promoted phagocytosis barely has substrate specificity (erythrocytes, *Escherichia coli*, live *Staphylococcus aureus*, and dying neuroblastoma cells). Our findings suggest that itaconate could potentially be used in the treatment of a broad range of phagocytosis-related diseases, supporting further development towards clinical application for the benefit of relevant clinical patients.

Introduction

The innate immune system is finely regulated to respond rapidly to a variety of stimuli, including pathogen (bacterial, fungal, and viral) invasion, host cell death, erythrocyte senescent, and erythrocyte escape from blood vessels.[1–3] Macrophages are congenital immune cells that play an important role in phagocytosis, antigen presentation, and cytokine production.[4] The dysfunction in phagocytosis of macrophages or microglia, the brain-resident macrophages, is associated with diseases occurring or worsening, such as chronic obstructive pulmonary disease,[5] atherosclerosis,[6] Alzheimer's disease,[7] and stroke.[8,9] In clinic, enhancing antibody-dependent macrophage phagocytosis has been successfully applied as a cancer immunotherapy.[10] Therefore, controlling macrophage phagocytosis is critical for maintaining health and treating diseases.[11]

Itaconate, a tricarboxylic acid cycle intermediate, is a product of the decarboxylation of *cis*-aconitate by immune-responsive gene 1 (Irg1) in the mitochondria.[12] Itaconate is an α, β-unsaturated dicarboxylic acid with mildly electrophilic properties, allowing it to act as a Michael acceptor to modify cysteine residue(s) in an alkylation reaction termed itaconation (also known as 2,3-dicarboxypropylation) on cysteine-containing proteins.[13–17] During the microbial invasion, itaconate directly inhibits the isocitrate lyase activity of *Pseudomonas indigofera* to limit pathogen growth,[18] and itaconyl-CoA, a breakdown product of itaconate metabolism, inhibits methylmalonyl-CoA mutase to restrict the growth of *Mycobacterium tuberculosis*.[19] Itaconate also potently attenuates intracellular replication of SARS-CoV2, Herpes Simplex Virus-1/2, Vaccinia Virus, and Zika Virus.[20,21] Moreover, itaconate exerts immunomodulatory effects by inhibiting enzymatic activity, such as succinate dehydrogenase[22] and ten-eleven translocation DNA dioxygenases[23] in macrophages. Therefore, itaconate is an essential regulator of macrophage activation, inflammation, and M1 polarization.[24] However, little is known about whether itaconate participates in macrophage phagocytosis and its underlying mechanisms.

Phagocytosis, the ingestion of bacteria or other material by phagocytes, is a highly conserved and complex process.[25] This process is mediated by the engagement of pattern recognition receptors, scavenger receptors, and Fc receptors.[26] CD36 is one of the well-studied class B scavenger receptors expressed on macrophages, monocytes, and microglia.[27] CD36 recognizes endogenous ligands, such as erythrocytes and apoptotic cells.[8,28] It also functions as a pattern recognition receptor on phagocytes, mediating engulfment and the elimination of foreign agents (bacterial and fungal pathogens).[29,30] Although both CD36 and itaconate are critical in development, maintaining tissue homeostasis, and host defense, whether CD36 is related to itaconate-participated functional regulation remains unknown.

Several disease models have been used to study phagocytosis, such as intracerebral hemorrhagic stroke (ICH),[8,9] peritonitis,[31] Alzheimer's disease,[32] and pneumonia.[33] ICH is associated with significant mortality and morbidity,[34,35] and the hematoma size is a well-established predictor of clinical outcomes in ICH patients.[36] Thus, enhancing microglia/macrophage (MMΦ) erythrophagocytosis and accelerating hematoma resolution is a legitimate therapeutic strategy for

ICH.[37] Bacterial peritonitis is another important disease related to phagocytosis regulation, which results from decreased phagocytosis and bactericidal capacity of host peritoneal macrophages,[38] and enhancing macrophage phagocytosis to reduce bacterial bioburden becomes a promising therapeutic option for the treatment of severe bacterial peritonitis. The goal of this study was to investigate whether itaconate modulates macrophage phagocytosis and its underlying mechanisms, thereby advancing future clinical translational studies.

Methods

Animals

Experiments in animals were performed according to the ARRIVE and ICLAS guidelines. All animals used in this study were bred and housed under specific-pathogen-free conditions at Capital Medical University. Mice were housed in a regulated environment (22 ± 2 °C, 55 ± 5% humidity, and 12:12-h light: dark cycle with lights on at 8:00 am) and received a standard diet. Food and water were accessible ad libitum. All procedures on mice were followed National Institutes of Health guidelines for care of animals. Anesthesia and euthanasia of animals were carried out based on the American Veterinary Medical Association Guidelines for the Euthanasia of Animals (2020).

C57BL/6 male mice (6- to 8-week-old, wildtype, WT) were obtained from Vital River (China). *Irg1*$^{-/-}$, *Irg1*$^{flox/flox}$, and *Cx3cr1*^{creERT} mice (all on a C57BL/6 background) were generated by Shanghai Model Organism Center, Inc (China). EGFP transgenic mice, which express enhanced EGFP in all tissues except erythrocytes and hair,[39] were used to visualize bone marrow-derived macrophages in time-lapse experiments and immunofluorescence staining.

To generate the *Irg1*$^{-/-}$ mice, CRISPR/Cas9 technology was used to repair the introduction of mutations by non-homologous recombination, resulting in the *Acod1* (*Irg1*) encoding protein reading frame-shifting and functional loss. To generate the *Irg1*$^{flox/flox}$ mice, the principle of homologous recombination was used to modify *Irg1* gene by flox through homologous recombination of fertilized eggs. Microglia/macrophage conditional knockout (cKO) mice were then produced by crossbreeding *Irg1*$^{flox/flox}$ mice with *Cx3cr1*^{creERT} mice (*Irg1*$^{flox/flox}$; *Cx3cr1*$^{creERT/+}$). When *Irg1*$^{flox/flox}$; *Cx3cr1*$^{creERT/+}$ mice became adults, we administered tamoxifen (T5648, Sigma–Aldrich, USA) 100 μL dissolved in corn oil (C805618, Macklin, China) at a concentration of 20 mg/mL once daily for 5 consecutive days to activate the creERT recombination. Age- and sex-matched littermates or WT mice were used as controls. The individual mouse was considered the experimental unit in this study. The PCR primer sequences for genotyping analysis were listed in Supplemental Table S2.

Ethics

All procedures on mice were approved by the Experimental Animal Ethics Committee (AEEI-2020-157 and AEEI-2023-013) of Capital Medical University, Beijing, China.

Cell cultures

Mouse bone marrow-derived macrophages were prepared from 6- to 8-week-old male mice and cultured as described previously.[8] Briefly, bone marrow cells from the mouse femur were flushed out with α-MEM (KGM11900-1, KeyGEN BioTECH, China). After lysing red blood cells (RBCs) with buffer (00-4300-54, Invitrogen, USA), cells were cultured in the medium supplemented with 10% fetal bovine serum (FBS; 10091148, Gibco, USA), 1% penicillin/streptomycin (KGY0023, KeyGEN BioTECH), and 20 ng/mL murine M-CSF (315-02-100, PeproTech, USA) for 7 d until use.

Mouse primary microglia were prepared from pups at postnatal days 0–1 and cultured as described previously.[8] Briefly, brain tissue was digested into single cells and cells were maintained in the DMEM/F12 medium (C11330500BT, Gibco) supplemented with 10% FBS and 1% penicillin/streptomycin *in vitro*. After 14 d culturing, cells were shaken at 200 rpm at 37 °C for 4 h to separate microglia from astrocytes. The medium was changed every 3 d until use.

Mouse macrophage cell line RAW264.7 and mouse neuroblastoma cell line N2A were maintained in DMEM medium (C11995500BT, Gibco) with 10% FBS and passaged every other day.

Phagocytosis assays

Time-lapse imaging

Briefly,[40] BMDMs extracted from EGFP mice were placed on a stage-top environmental chamber that maintained the cells at 37 °C in 5% CO_2 and was mounted onto a Zeiss inverted microscope (LSM880, Zeiss, Germany). Cells were incubated with pH-sensitive latex beads (4 μm, P35364, Invitrogen) and nuclear dye Hoechst 33342 (C0031, Solarbio, China). Z-stack images were captured every 3–4 min for a total duration of 1 h. Images and videos were obtained by the Zeiss imaging software and analyzed using the ImageJ software (NIH, USA).

Flow cytometry

Briefly,[41] pH-sensitive latex beads (pHrodo Red, Excitation/Emission = 560/585 nm) were incubated with BMDMs for 20 min and unengulfed beads were washed. BMDMs were digested by 0.25% trypsin (KGY0012, KeyGEN BioTECH), washed, and analyzed with an LSRFortessa SORP cytometer (BD Biosciences, USA). Dead cells were distinguished with 7-Aminoactinomycin D (7AAD; 00-6993-50, eBioscience, USA). Unengulfed BMDMs (7AAD^{-}PE^{-}) were used as a negative control. FlowJo software V10 (SU, USA) was used to analyze the results. The engulfment (%) was calculated by the

percentage of beads-engulfing BMDMs ($7AAD^-PE^+$) in all live BMDMs ($7AAD^-$). The number of engulfed beads was calculated by the mean fluorescence intensity of beads in beads-engulfing BMDMs ($7AAD^-PE^+$).

Immunofluorescence staining

For *in vitro* experiments, briefly,[42] pH-sensitive latex beads, pH-sensitive *Escherichia coli* (*E. coli*; P35361, Invitrogen), PKH26-labeled RBCs, or propidium iodide (PI)-labeled dying cancer cells were incubated with cells for 20 min, respectively. Phagocytes were washed and fixed with 4% paraformaldehyde (PFA; P1110, Solarbio), washed, and immunostained. Z-stack images were captured with a confocal microscope (TCS SP8 STED, Leica, Germany). The beads number was calculated by the number of engulfed beads per phagocyte, and the engulfment (%) was calculated by the percentage of engulfed phagocytes in total phagocytes in each field. For *in vivo* experiments, briefly,[8] PKH26-labeled RBCs (1×10^6) in 2 μL phosphate buffered solution (PBS; P1010, Solarbio) were injected into the left mouse striatum at 0.4 μL/min (coordinates: x = 2.0 mm, y = 0.8 mm, z = −3.15 mm). Mice were sacrificed and brain sections were used for immunofluorescence staining. Four random perihematomal areas on 6 brain sections at 3 slides per animal were used and quantified by ImageJ software. The RBC number was calculated by the number of engulfed RBCs per microglia/macrophage.

Intracerebral hemorrhage mouse model

As previously described,[43] we used collagenase to induce the ICH mouse model. Briefly, mice were deeply anesthetized with isoflurane (mixture of 70% N_2O and 30% O_2; 3% induction, 1–2% maintenance). A burr hole was made in the left striatum (coordinates: x = 2.0 mm, y = 0.8 mm, z = −3.15 mm). Next, 0.5 μL of collagenase VII-S (0.1 U/μL, Sigma–Aldrich) was injected at a speed of 0.1 μL/min. The body temperature of mice was maintained near normothermia (37.0 °C) during surgery with a heating blanket (RWD, China). All efforts were made to minimize the number of animals used and ensure minimal suffering. Body weight, rectal temperature, and survival rate were recorded for each mouse before and after surgery until the endpoint of experiments.

Acute bacterial peritonitis mouse model

As previously described,[44] *Staphylococcus aureus* (*S. aureus*) was grown in Luria Broth (LB) media and shaken overnight at 37 °C. *S. aureus* density was determined using an ultraviolet–visible spectrophotometer (Nanodrop 2000, Thermo Fisher Scientific, USA) and the corresponding colony-forming units (CFU) were determined on LB agar plates. Viable 1×10^9 CFU *S. aureus* resuspended in 1 mL of LB was injected into the peritoneal cavity (*i.p.*). Body weight and survival rate were recorded for each mouse before and after *S. aureus* injection. All experiments performed using *S. aureus* were performed in ClassII Biohazard facilities.

Statistical analysis

Animals and cell cultures for each group were randomized with the website www.randomization.com. Each animal was randomly assigned to a cage from all cages, and the order of the trials was randomized daily. Treatment, data collection, and data analyses were blinded by using different investigators or by masking sample labels. Three or more independent experiments were performed for all experiments. For the pooled analysis of results from different independent replications, all mice and independent *in vitro* experiments from the same experimental group were pooled and a new statistical comparison was performed for the entire pooled experiment, as was done for the individual replications.[45] A power analysis based on previous studies,[43,46,47] and pilot data indicated that 8 mice per group would provide at least 80% power for detecting a 20% decrease in neurologic deficits at $\alpha = 0.05$ (2-sided). Sample sizes were excluded the animals which were died or euthanized. To be specific, the ICH mice that died or had a neurological deficit score higher than 20 at 24 h after surgery were euthanized and excluded from the analysis. And the peritonitis animals with obvious abnormal behavior (*i.e.*, exceeding 2 times the standard deviation) were excluded. Data were presented as mean ± SD or displayed using violin plots (medians, quartiles Q25-Q75 and 95% confidence intervals). Mean value was the average data obtained from all animals (*in vivo* experiments) or from three or more independent experiments (*in vitro* experiments). All data analysis was performed using GraphPad Prism 8.0.2 (263) Software. For all datasets, the normality was assessed using the Shapiro–Wilk test, and the parametric or non-parametric tests were used accordingly. For comparisons between two groups with normal distribution, unpaired two-tailed Student's *t*-test followed by Welch's correction was performed. For comparison of more than two groups, ANOVA was used with correction for multiple comparisons tests for parametric-distributed datasets and the Kruskal–Wallis test with Dunn's correction for non-parametric-distributed datasets. To be specific, One-way ANOVA followed by Tukey's multiple comparisons test or Dunnett's multiple comparisons tests, and Two-way ANOVA followed by Sidak's multiple comparisons test or Tukey's multiple comparisons tests were used to determine where those differences occurred. The criterion for statistical significance was $p < 0.05$. All exact p values were presented in Supplemental Table S3.

Role of funders

The funding sources were not involved in study design, data collection, data analyses, interpretation, or writing of report.

Results

Irg1/itaconate axis promotes macrophage phagocytosis

We extracted bone marrow-derived macrophages (BMDMs) from wild-type (WT) mice (Supplemental Fig. S1a), treated them with itaconate derivative 4-octyl itaconate (4-OI) or vehicle, and performed RNA-sequencing (RNA-seq) analysis (n = 3, Fig. 1a). Gene Set Enrichment Analysis (GSEA) showed that regulation of the phagocytosis-related genes was significantly enriched in 4-OI-treated macrophages (n = 3, Fig. 1b and Supplemental Table S1). We verified the RNA-seq results with real-time RT-PCR (n = 3, $p < 0.05$ *vs.* Veh, Fig. 1c). We next incubated macrophages with pH-sensitive latex beads to assess the changes in phagocytosis. Both itaconate (1 mM) and 4-OI (120 μM) significantly increased the total amount of phagocytosed beads and the percentage of beads-engulfing macrophages (n = 3, $p < 0.05$ *vs.* Veh, Supplemental Fig. S1b–g). The time-lapse recording revealed that itaconate and 4-OI also increased the beads-engulfing speed and ability of macrophage phagocytosis (n = 8–52, $p < 0.01$ *vs.* Veh, Fig. 1d–f and Supplemental Videos S1–S3). Of note, the phagocytosis-enhancing effective dosages of itaconate and 4-OI didn't induce cell death (n = 4 or 5, $p > 0.05$ *vs.* Veh, Supplemental Fig. S1h–k).

Immune-responsive gene 1 (Irg1) converts *cis*-aconitate to itaconate. To further confirm *Irg1*'s role in macrophage phagocytosis, we generated $Irg1^{-/-}$ mice (Supplemental Fig. S2a) and observed the depletion of Irg1 by real-time RT-PCR (n = 3, $p < 0.001$ *vs.* $Irg1^{+/+}$, Supplemental Fig. S2b) and Western blotting (Supplemental Fig. S2c), and the depletion of itaconate in $Irg1^{-/-}$ BMDMs by high-performance liquid chromatography (HPLC) analysis (Supplemental Fig. S2d). As reported elsewhere,[48] we also found that deficiency of *Irg1* didn't affect macrophage maturation, glycolysis, and mitochondrial respiration (n = 3, $p > 0.05$ *vs.* $Irg1^{+/+}$, Supplemental Fig. S2e–h). As expected, BMDMs extracted from $Irg1^{-/-}$ mice showed impaired phagocytic activity (n = 4, $p < 0.05$ *vs.* $Irg1^{+/+}$, Fig. 1g–i and Supplemental Fig. S2i–k), and both itaconate and 4-OI rescued this dysfunction (n = 4, $p < 0.05$ *vs.* Veh, Fig. 1g–i and Supplemental Fig. S2i–k), whereas *Irg1* overexpression increased phagocytosis of WT BMDMs (n = 3, $p < 0.001$ *vs.* Vector, Supplemental Fig. S2l and m). We further incubated macrophages with *Escherichia coli* (*E. coli*), red blood cells (RBCs), or dying cancer cells (CCs). *Irg1* deficiency markedly attenuated the phagocytosis of *E. coli*, RBCs, and dying CCs (n = 4, $p < 0.05$ *vs.* $Irg1^{+/+}$, Fig. 1j and k), while the addition of itaconate/4-OI promoted engulfment in both $Irg1^{+/+}$ and $Irg1^{-/-}$ BMDMs (n = 4, $p < 0.05$ *vs.* Veh, Fig. 1j and k). These data suggest that Irg1/itaconate axis plays an important role in the regulation of macrophage phagocytosis.

Irg1/itaconate axis enhances macrophage phagocytosis by activating the Keap1/Nrf2/CD36 axis

Peroxisome proliferator-activated receptor (PPAR)-γ and nuclear factor erythroid 2-related factor 2 (Nrf2) are the most studied phagocytosis-related transcription factors.[42,49,50] Kyoto Encyclopedia of Genes and Genomes (KEGG) and violin plot analyses showed that both PPAR and Nrf2 signaling pathway-related genes were enriched in the 4-OI-treated cells (n = 3, Supplemental Fig. S3a–c). Treating cells with PPARγ inhibitor T0070907 did not inhibit 4-OI-promoted phagocytosis (n = 3, $p > 0.05$ 4-OI+ T0070907 *vs.* 4-OI+Veh, Supplemental Fig. S3d), while pharmacologic inhibition of Nrf2 transcriptional activity with ML385 decreased the 4-OI-enhanced phagocytosis significantly (n = 3, $p < 0.001$ 4-OI+ML385 *vs.* 4-OI+Veh, Supplemental Fig. S3e). These results suggest that the Nrf2 signaling pathway plays an important role in Irg1/itaconate axis-regulated macrophage phagocytosis.

Kelch-like ECH-associated protein 1 (Keap1) binds to Nrf2 in cytosol and represses Nrf2 nuclear translocation.[51] Itaconate has electrophilic properties and directly alkylates cysteine residue on the Keap1 to promote Nrf2 transcription of anti-inflammatory and antioxidative genes.[13] As expected, 4-OI did not alter the mRNA levels of *Keap1* or *Nrf2* (n = 6, $p > 0.05$ *vs.* Veh, Supplemental Fig. S3f), but 4-OI significantly increased the nuclear translocation of Nrf2 detected by immunofluorescence staining and Western blotting (n = 3, Fig. 2a and b). We next analyzed Nrf2-transcripting genes by using chromatin immunoprecipitation-sequencing (ChIP-seq) assays. A total of 192 differential binding sites were identified, and 4-OI induced binding of Nrf2 to the transcription start site of target genes (Fig. 2c). Venn diagrams showed there were 44 overlapped differentially expressed genes (4-OI *vs.* Veh) between results gained from ChIP-seq and RNA-seq analyses, and they were mainly involved in oxidative stress and redox pathway, cellular response to oxidative stress, carboxylic acid transmembrane transport, and mitotic cell cycle process (Fig. 2d and Supplemental Fig. S3g). Among these, genes encoding the scavenger receptor CD36 and proton-coupled divalent metal ion transporter SLC11A1 were the overlapped phagocytosis-related genes between ChIP-seq and RNA-seq assays (Fig. 2d). CD36 neutralizing antibodies largely blocked 4-OI-enhanced phagocytosis in WT BMDMs (n = 4, $p < 0.01$ 4-OI+Ab-CD36 *vs.* 4-OI+IgA, Fig. 2e), whereas *Slc11a1* silencing had modest effects on it (n = 4, $p > 0.05$ 4-OI+si*Slc11a1* *vs.* 4-OI+si*Ctrl*, Supplemental Fig. S3h and i). In addition, ChIP-seq density tracking and our ChIP assay showed 4-OI enhanced the binding of Nrf2 on the transcription start site of *Cd36* (Fig. 2f and g). Meanwhile, addition of 4-OI also induced *Cd36* overexpression (n = 5, $p < 0.01$ *vs.* Veh, Fig. 2h–j).

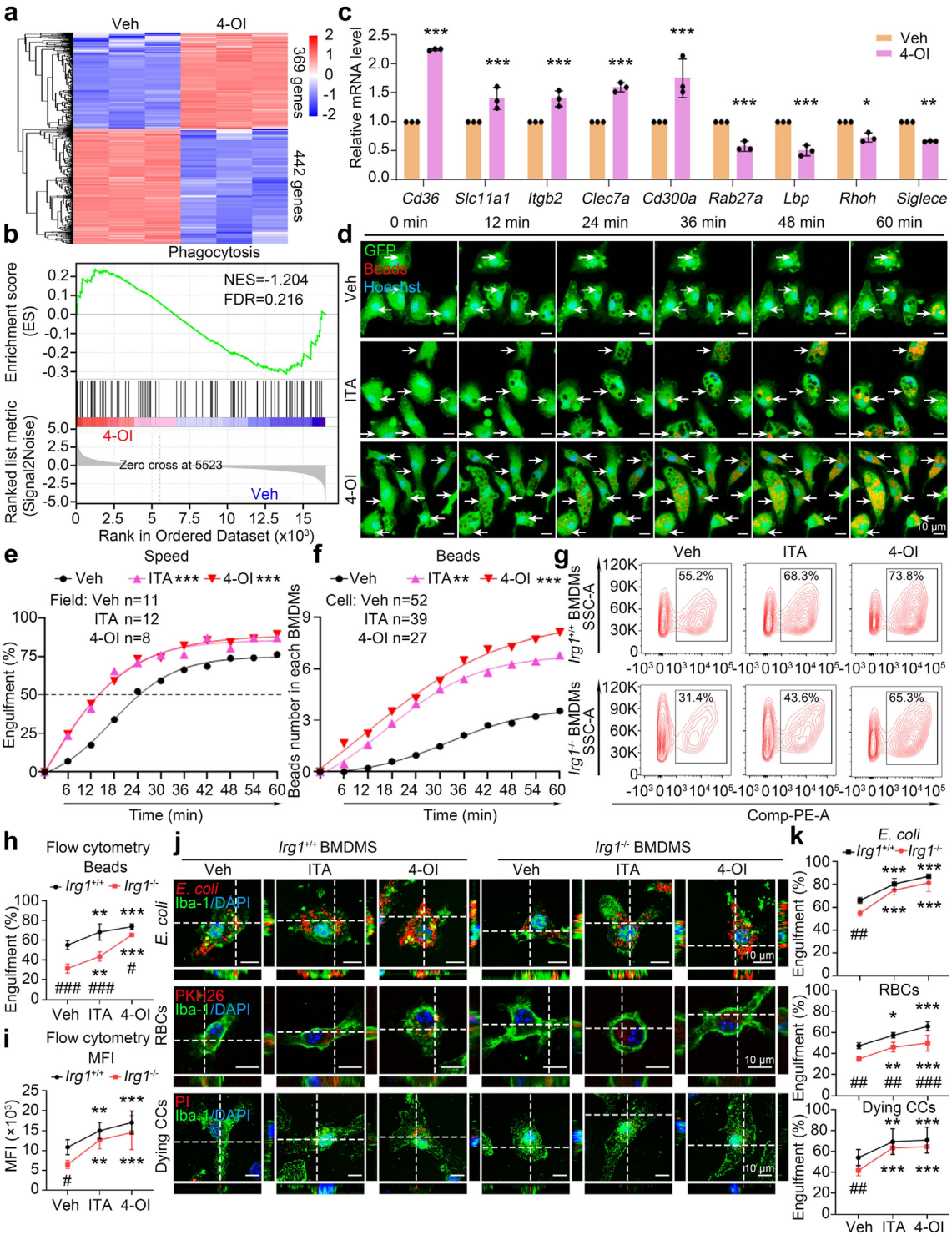

Fig. 1: **Irg1/itaconate axis promotes macrophage phagocytosis.** (**a** and **b**) Bone marrow-derived macrophages (BMDMs) isolated from C57BL/6 (WT) mice were treated as indicated to perform RNA-seq analysis. Hierarchical clustering analysis of differentially expressed genes (a) and a GSEA analysis of phagocytosis pathway (b) are shown. (**c**) The mRNA levels of phagocytosis-related genes in WT BMDMs were analyzed using real-time RT-PCR after treatment 8 h. *GAPDH* serves as an internal control. n = 3, *$p < 0.05$, **$p < 0.01$, ***$p < 0.001$ *vs.* Veh. (**d**–**f**) BMDMs isolated from EGFP mice were exposed to indicated treatments before incubated with the pH-sensitive latex beads. The time-lapse recording was performed. Nuclei were stained with Hoechst dye. White arrows indicate beads-engulfing macrophages. Fields calculated for evaluating

To confirm itaconate upregulated *Cd36* expression through Keap1 itaconation, we mutated candidate cysteines (151 and 288) to serines (Keap1^{C151S} and Keap1^{C288S}) as literature showed that these two are the most important itaconation sites[13,52] (Supplemental Fig. S3j and k). 4-OI-induced Nrf2 nuclear translocation (n = 3, Fig. 3a and b) and *Cd36* expression (n = 3, $p > 0.05$ Keap1^{C151S} 4-OI *vs.* Keap1^{C151S} Veh, Fig. 3c–e) were markedly attenuated in Keap1^{C151S} cells. Interestingly, we noticed that Keap1^{C288S} promoted Nrf2 nuclear translocation even without 4-OI treatment (n = 3, Fig. 3a and b), but this mutation did not affect 4-OI increased *Cd36* expression (n = 3, $p < 0.01$ Keap1^{C288S} 4-OI *vs.* Keap1^{C288S} Veh, Fig. 3c–e). These results indicate that cysteine 151 is the most important itaconated cysteine on Keap1 in both activating Nrf2 for anti-inflammation[13,53–55] and phagocytosis promotion. To further confirm the role of Nrf2 in promoting *Cd36* overexpression, we transfected WT BMDMs with *Nrf2* siRNA or control siRNA.[56] Real-time RT-PCR results showed that Nrf2 mRNA level was significantly downregulated after *Nrf2* siRNA transfection (n = 4, $p < 0.01$ *vs.* si*Ctrl*, Supplemental Fig. S3l), and 4-OI-promoted *Cd36* overexpression was significantly blocked by *Nrf2* siRNA transfection (n = 5, $p < 0.001$ 4-OI+si*Nrf2* *vs.* 4-OI+si*Ctrl*, Fig. 3f). Additionally, Nrf2 inhibitor ML385 (n = 4 or 3, $p < 0.05$ 4-OI+ML385 *vs.* 4-OI+Veh, Fig. 3g–j), but not PPAR-γ inhibitor T0070907 (n = 3, $p > 0.05$ 4-OI+T0070907 *vs.* 4-OI+Veh, Supplemental Fig. S3m), decreased the 4-OI-upregulated *Cd36* overexpression.

Collectively, these results indicate that itaconate regulates macrophage phagocytosis by regulating the Keap1/Nrf2/CD36 axis, but not through the PPARγ signaling pathway (Fig. 3k).

Irg1/itaconate axis enhances erythrophagocytosis of MMΦ and improves acute outcomes in an ICH mouse model

Intracerebral hemorrhagic stroke (ICH) is an established disease model to study macrophage phagocytosis.[9,57] The activated infiltrating macrophages are one of the most important phagocytes to engulf RBCs, thereby promoting hematoma clearance and brain repair after ICH.[58,59] Heme is a degradation product of RBCs and hemin has been commonly used to mimic ICH toxicity *in vitro*.[60] Hemin slightly increased the total amount of engulfed beads (n = 14, $p < 0.05$ *vs.* Veh, Fig. 4a and b; n = 3, Supplemental Fig. S4a and c, Supplemental Videos S4 and S5) and the percentage of phagocytic macrophages (n = 4, $p < 0.01$ *vs.* Veh, Supplemental Fig. S4a and b, Supplemental Videos S4 and S5), but not the phagocytosis speed (n = 4, $p > 0.05$ *vs.* Veh, Fig. 4a and c, Supplemental Videos S4 and S5). Among the hemin-induced differentially regulated genes which were assessed with RNA-seq, *Irg1* was only slightly upregulated (n = 3, Fig. 4d and Supplemental Fig. S4d). We further confirmed the upregulation of Irg1 in macrophages (n = 5, $p < 0.05$ *vs.* Veh, Fig. 4e and f). These results suggest that Irg1/itaconate axis may be involved in hemin-induced macrophage phagocytosis. Hemin only marginally activated the Irg1/itaconate axis, and enhancing this axis may further augment its phagocytosis capacity.

Consistent with slightly increased Irg1 levels, hemin also slightly increased the Nrf2 protein levels in both whole-cell lysate and nuclear fraction, and co-treating cells with 4-OI and hemin dramatically enhanced Nrf2 protein levels, especially in nuclear fraction (n = 3, Fig. 4g and h). *Cd36* expression was also significantly elevated in the co-administration of 4-OI with hemin (n = 9 or 4, $p < 0.001$ Hemin+4-OI *vs.* Hemin+Veh, Fig. 4i and j). Additionally, co-administration of 4-OI and hemin promoted phagocytosis in both *Irg1*$^{+/+}$ and *Irg1*$^{-/-}$ BMDMs assessed by incubating with RBCs (n = 3, $p < 0.01$ Hemin+ITA, Hemin+4-OI *vs.* Hemin+Veh, Fig. 5a and b) or pH-sensitive latex beads (n = 3 or 4, $p < 0.01$ Hemin+ITA, Hemin+4-OI *vs.* Hemin+Veh, Fig. 5c–g). Moreover, the CD36 neutralizing antibody effectively blocked 4-OI-enhanced phagocytosis in hemin-treated cells (n = 4, $p < 0.001$ Hemin+4-OI+Ab-CD36 *vs.* Hemin+4-OI+IgA, Fig. 5h and i). These data indicate that hemin induces phagocytosis mainly through upregulation of CD36 in an itaconate-dependent or -independent manner, enhancing Irg1/itaconate levels certainly augments macrophage engulfment even incubating with hemin.

Microglia, as the resident macrophages in brain tissue, are also primary phagocytes post-ICH,[61] but they may not share identical regulatory mechanisms in phagocytosis.[62] We treated primary microglia that were isolated from WT mouse brain with hemin (Supplemental Fig. S4e). Hemin upregulated the

engulfment (%): Veh n = 11, ITA n = 12, 4-OI n = 8. BMDMs calculated for evaluating beads number: Veh n = 52, ITA n = 39, 4-OI n = 27. $^{**}p < 0.01$, $^{***}p < 0.001$ *vs.* Veh. Scale bar = 10 μm. (**g–i**) Indicated BMDMs were treated as indicated and incubated with pH-sensitive latex beads, and then flow cytometry was performed. n = 4, $^{**}p < 0.01$, $^{***}p < 0.001$ *vs.* corresponding Veh; #$p < 0.05$, ###$p < 0.001$ *vs.* *Irg1*$^{+/+}$ BMDMs. MFI: Mean fluorescence intensity. (**j** and **k**) Indicated BMDMs were incubated with pH-sensitive *Escherichia coli* (*E. coli*), PKH26-labeled red blood cells (RBCs), or PI-labeled dying cancer cells (CCs) respectively. n = 4, $^{*}p < 0.05$, $^{**}p < 0.01$, $^{***}p < 0.001$ *vs.* corresponding Veh; ##$p < 0.01$, ###$p < 0.001$ *vs.* *Irg1*$^{+/+}$ BMDMs. Scale bar = 10 μm. Data are presented as mean ± SD. (**c**) Two-way ANOVA followed Sidak's multiple comparisons test. (**e** and **f**) Two-way ANOVA followed Tukey's multiple comparisons test. (**h**, **i**, and **k**) Two-way ANOVA followed Tukey's or Sidak's multiple comparisons test.

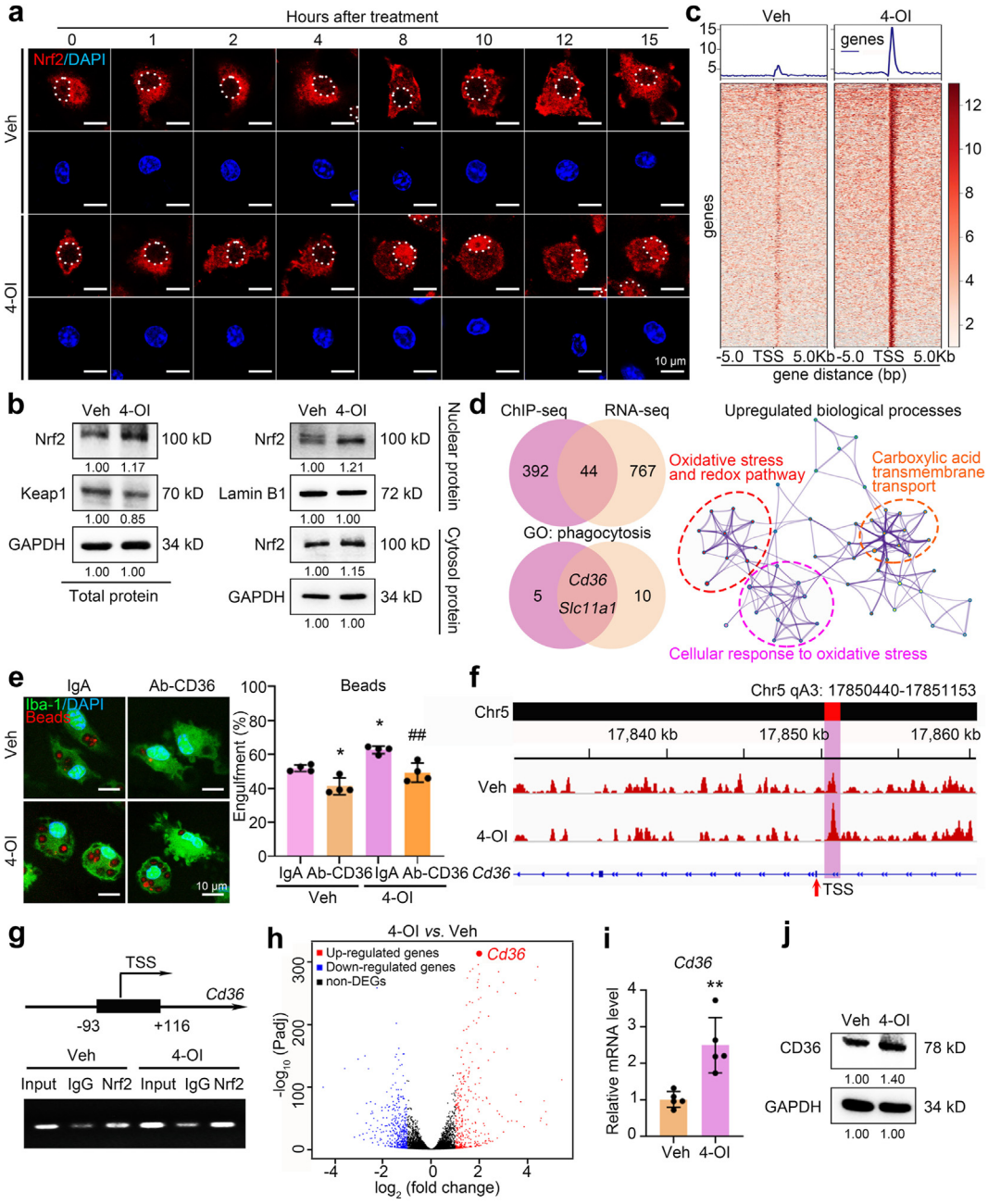

Fig. 2: **Irg1/itaconate axis increases the nuclear translocation of Nrf2, which increases *Cd36* transcription.** (**a**) WT BMDMs were treated with 4-OI or vehicle at different time points. Immunofluorescence staining was performed with Nrf2 antibodies. The dash line indicates the location of nuclei. Scale bar = 10 μm. (**b**) RAW264.7 cells were treated with 4-OI or vehicle for 8 h, and Western blotting was performed. GAPDH serves as an internal control of the total protein and cytosol portion. Lamin B1 serves as an internal control of the nuclear portion. (**c**) RAW264.7 cells were treated as indicated for 8 h to perform ChIP-seq analysis using Nrf2 antibodies. A heatmap of differentially binding sites is shown. TSS: transcription start site. (**d**) Venn diagram and network plot show the overlapped differential expressed genes and upregulated biological processes between RNA-seq and ChIP-seq. (**e**) WT BMDMs were treated as indicated and incubated with pH-sensitive latex beads. Immunofluorescence staining was performed using Iba-1 antibodies. n = 4, $^{*}p < 0.05$ *vs.* Veh+IgA; $^{\#\#}p < 0.01$ *vs.* 4-OI+IgA. Scale bar = 10 μm. (**f**) The density tracking of Nrf2 binding on *Cd36* with ChIP-seq analysis is shown. (**g**) ChIP assay followed by agarose gel electrophoresis was performed using Nrf2 antibodies or IgG in RAW264.7 cells. (**h**) The differential expressed genes are shown with a volcano plot in WT BMDMs detected using RNA-seq. *Cd36* is marked in red. n = 3. (**i** and **j**) The expression levels of *Cd36* in WT BMDMs were examined using real-time RT-PCR (i) and Western blotting (j). GAPDH serves as an internal control. n = 5, $^{**}p < 0.01$ *vs.* Veh. Data are presented as mean ± SD. (**e**) One-way ANOVA followed Tukey's multiple comparisons test. (**i**) Two-tailed Student's *t*-test followed by Welch's correction.

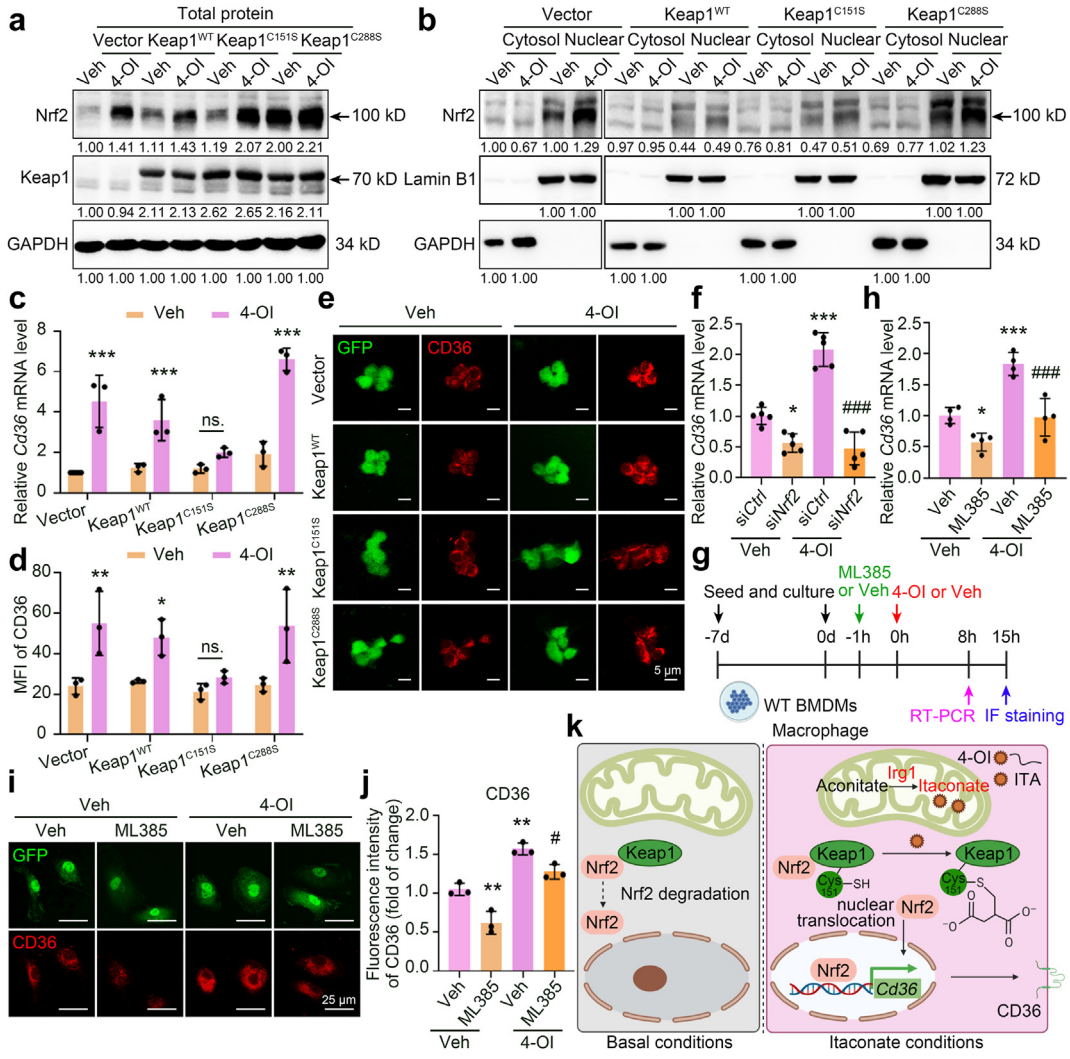

***Fig. 3:* Irg1/itaconate axis regulates macrophage phagocytosis by regulating the Keap1/Nrf2/CD36 axis.** (**a**–**c**) RAW264.7 cells infected with indicated mutates were treated as indicated for 8 h. (a, b) Western blotting was performed. GAPDH serves as an internal control of the total protein and cytosol portion. Lamin B1 serves as an internal control of the nuclear portion. (c) The mRNA level of *Cd36* was assessed with real-time RT-PCR. *GAPDH* serves as an internal control. n = 3, ***p < 0.001 *vs.* Veh. ns., not significant *vs.* Veh. (**d** and **e**) RAW264.7 cells infected with different mutates (with EGFP tags) were treated as indicated for 15 h. The protein level of CD36 was assessed with immunofluorescence staining. n = 3, *p < 0.05, **p < 0.01 *vs.* Veh. ns., not significant *vs.* Veh. Scale bar = 5 μm. (**f**) *Nrf2* siRNA or control siRNA was transfected respectively into WT BMDMs. The mRNA level of *Cd36* was assessed with real-time RT-PCR. n = 5, *p < 0.05, ***p < 0.001 *vs.* Veh+si*Ctrl*; ###p < 0.001 *vs.* 4-OI+si*Ctrl*. (**g**) Schematic procedure of drug treatment. (**h**) WT BMDMs were treated as indicated for 8 h and mRNA was extracted to perform real-time RT-PCR. *GAPDH* serves as an internal control. n = 4, *p < 0.05, ***p < 0.001 *vs.* Veh+Veh; ###p < 0.001 *vs.* 4-OI+Veh. (**i** and **j**) BMDMs were isolated from EGFP mice and treated as indicated for 15 h. The immunofluorescence staining using CD36 antibodies was performed. n = 3, **p < 0.01 *vs.* Veh+Veh; #p < 0.05 *vs.* 4-OI+Veh. Scale bar = 25 μm. (**k**) Schematic diagram of Irg1/itaconate axis promoting macrophage phagocytosis by regulating the Keap1/Nrf2/CD36 axis. Data are presented as mean ± SD. (**c** and **d**) Two-way ANOVA followed Sidak's multiple comparisons test. (**f**, **h**, and **j**) One-way ANOVA followed Tukey's multiple comparisons test.

expression level of *Irg1* (n = 4, p < 0.001 *vs.* Veh, Supplemental Fig. S4f and g). 4-OI also promoted microglia to engulf beads even under hemin incubation (n = 3, p < 0.01 Hemin+4-OI *vs.* Hemin+Veh, Supplemental Fig. S4h), and 4-OI-enhanced phagocytosis in hemin-treated cells was abolished by administering Nrf2 inhibitor ML385 (n = 3, p < 0.01 Hemin+4-OI+ML385 *vs.* Hemin+4-OI+Veh, Supplemental Fig. S4i) and CD36 neutralizing antibodies (n = 3, p < 0.001 Hemin+4-OI+Ab-CD36 *vs.* Hemin+4-OI+IgA, Supplemental Fig. S4j). These results suggest that Irg1/itaconate axis may promote MMΦ phagocytosis *via* the

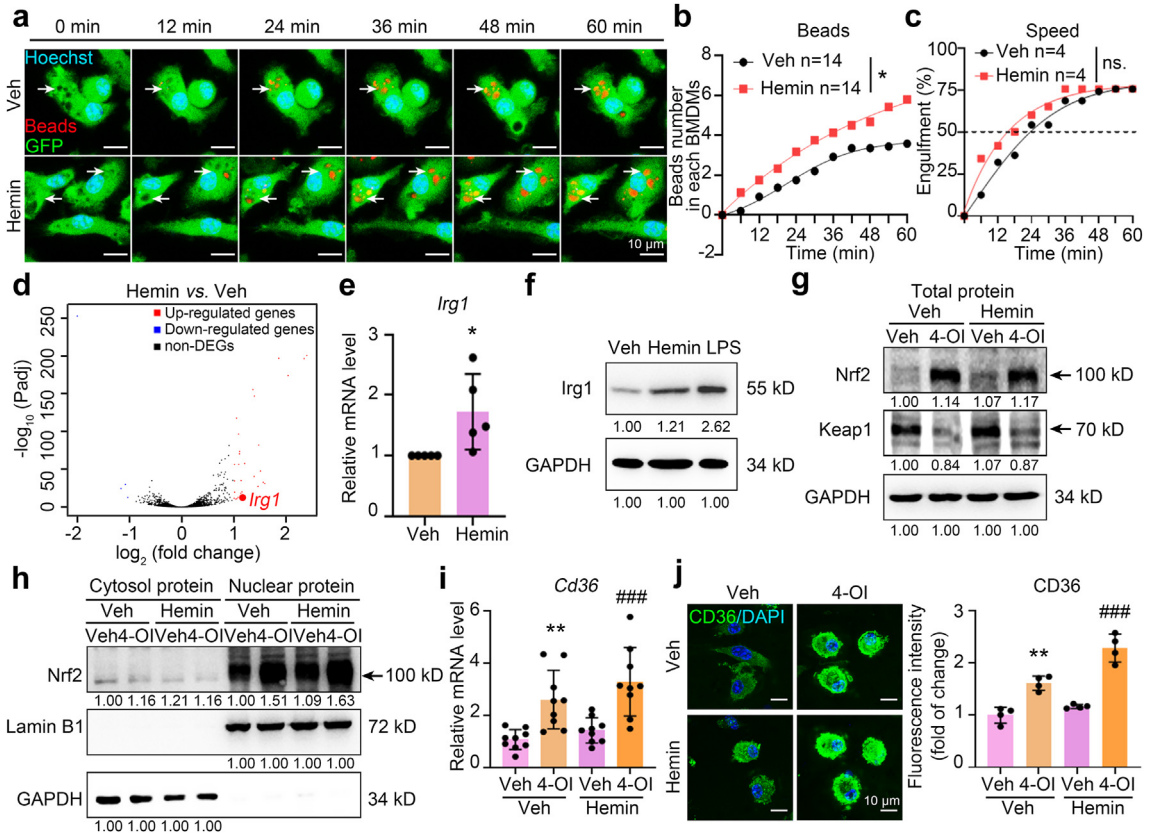

Fig. 4: **Irg1/itaconate axis promotes macrophage phagocytosis via Nrf2/CD36 axis after ICH *in vitro*.** (**a–c**) BMDMs isolated from EGFP mice were exposed to different treatments for 12 h. The time-lapse recording was performed after adding the pH-sensitive latex beads. The nuclei were stained with Hoechst dye. White arrows indicate beads-engulfing macrophages. BMDMs calculated for evaluating beads number: Veh n = 14, Hemin n = 14. Fields calculated for evaluating engulfment (%): Veh n = 4, Hemin n = 4. Scale bar = 10 μm. (**d**) WT BMDMs were treated as indicated for 8 h, and RNA-seq analysis was performed. A volcano plot showed the differential expressed genes. *Irg1* is marked in red. n = 3. (**e** and **f**) The levels of mRNA (e) and protein (f) of *Irg1* in WT BMDMs were examined with real-time RT-PCR and Western blotting. GAPDH serves as an internal control. n = 5, $^{*}p < 0.05$ *vs.* Veh. (**g** and **h**) Proteins were extracted from the RAW264.7 cells which were treated as indicated, and the Western blotting was performed. GAPDH serves as an internal control of the total protein and cytosol portion, and Lamin B1 serves as an internal control of the nuclear portion. (**i** and **j**) The mRNA levels of *Cd36* (i, n = 9) and protein levels of CD36 (j, n = 4) were assessed with real-time RT-PCR and immunofluorescence staining. $^{**}p < 0.01$ *vs.* Veh+Veh; $^{###}p < 0.001$ *vs.* Hemin+Veh. Scale bar = 10 μm. Data are presented as mean ± SD. (**b** and **c**) Two-way ANOVA followed Tukey's multiple comparisons test. (**e**) Two-tailed Student's *t*-test followed by Welch's correction. (**i** and **j**) One-way ANOVA followed Tukey's multiple comparisons test.

same Nrf2/CD36 axis. In addition, 4-OI also decreased the inflammatory response in the *in vitro* cell model of ICH (n = 3 or 6, $p < 0.001$ Hemin+4-OI *vs.* Hemin+Veh, Supplemental Fig. S4k–n), which was consistent with the role of itaconate in decreasing inflammatory factor production in diseases such as ischemia-reperfusion injury,[22] lipopolysaccharide (LPS)-induced lethal endotoxemia,[15,23] and bacterial endophthalmitis.[63]

To investigate the effects of *Irg1* on MMΦ after ICH *in vivo*, we generated conditional *Irg1* knockout mice by crossing $Irg1^{flox/flox}$ with $Cx3cr1^{creERT/+}$ mouse strains (refers as *Irg1* cKO) (Supplemental Fig. S5a–d). We first stereotactically injected PKH26 dye-stained RBCs into the striata of mice. Compared with the control mice (*Irg1* flox), MMΦ (Iba1^{+} cells) in *Irg1* cKO mice engulfed fewer RBCs in the perihematomal region (n = 5 animals including 10 fields, $p < 0.05$ *vs.* *Irg1* flox, Fig. 6a). Next, we subjected mice to the collagenase injection which is the most well-established *in vivo* ICH model (Fig. 6b). *Irg1* cKO mice exhibited a significantly larger hematoma volume on 5 d post-ICH (n = 10 animals, $p < 0.05$ *vs.* *Irg1* flox, Fig. 6c). The delayed hematoma clearance in *Irg1* cKO mice ultimately translated into aggravated neurologic and motor dysfunction (n = 10 animals, $p < 0.05$ *vs.* *Irg1* flox, Fig. 6d). Importantly, *Irg1* cKO and control mice had a comparable number (n = 8 animals, $p > 0.05$ *vs.* *Irg1* flox, Supplemental Fig. S5e and f) and soma area of MMΦ in the perihematomal region

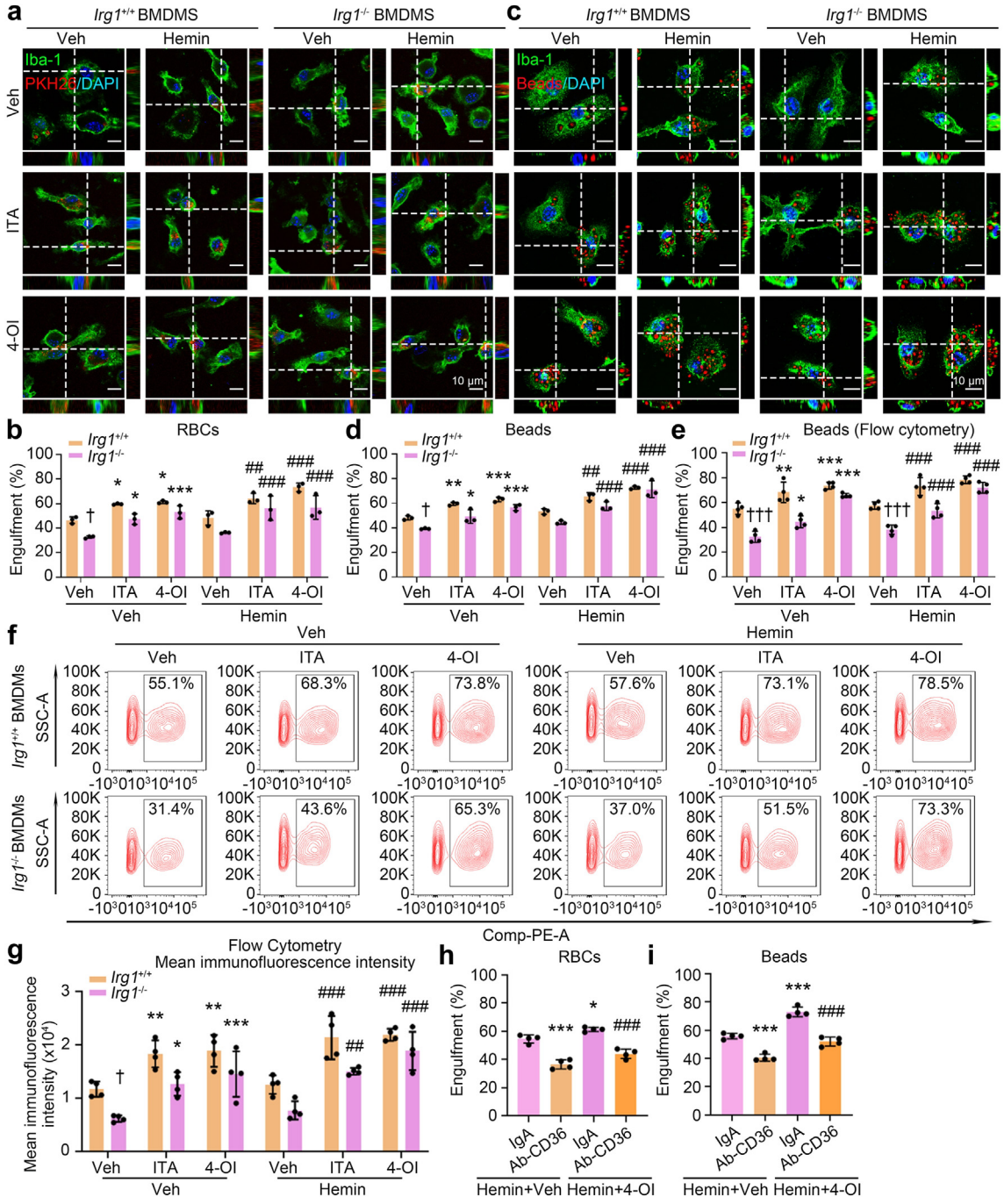

Fig. 5: **Irg1/itaconate axis promotes macrophage phagocytosis after ICH *in vitro*.** (**a** and **b**) BMDMs obtained from *Irg1*$^{+/+}$ or *Irg1*$^{-/-}$ mice were treated as indicated for 15 h and incubated with PKH26-labeled RBCs. Then, immunofluorescence staining was performed using Iba-1 antibodies. n = 3, *p < 0.05, ***p < 0.001 *vs.* corresponding Veh; ##p < 0.01, ###p < 0.001 *vs.* corresponding Hemin; †p < 0.05 *vs.* *Irg1*$^{+/+}$ BMDMs. Scale bar = 10 μm. (**c** and **d**) The *Irg1*$^{+/+}$ and *Irg1*$^{-/-}$ BMDMs were treated as indicated and incubated with pH-sensitive latex beads. Immunofluorescence staining was performed with Iba-1 antibodies. n = 3, *p < 0.05, **p < 0.01, ***p < 0.001 *vs.* corresponding Veh; ##p < 0.01, ###p < 0.001 *vs.* corresponding Hemin; †p < 0.05 *vs.* *Irg1*$^{+/+}$ BMDMs. Scale bar = 10 μm. (**e**–**g**) The *Irg1*$^{+/+}$ and *Irg1*$^{-/-}$ BMDMs were treated as indicated and incubated with pH-sensitive latex beads. The flow cytometry was performed. n = 4, *p < 0.05, **p < 0.01, ***p < 0.001 *vs.* corresponding Veh; ##p < 0.01, ###p < 0.001 *vs.* corresponding Hemin; †p < 0.05, †††p < 0.001 *vs.* *Irg1*$^{+/+}$ BMDMs. (**h**) The WT BMDMs were

(n = 65–80 MMΦ from 7 animals, $p > 0.05$ *vs.* *Irg1* flox, Supplemental Fig. S5e and g), indicating that impaired hematoma resolution was not due to the dysfunction of migration/recruitment/activation of MMΦ after ICH.

Moreover, administration of sodium itaconate (Na-ITA) into *Irg1* cKO mice rescued hematoma clearance deficiency (n = 7 animals, $p < 0.05$ *vs.* Veh, Fig. 6e) and neurobehavior dysfunction (n = 9 animals, $p < 0.05$ *vs.* Veh, Fig. 6f), and 4-OI administration into WT mice accelerated hematoma clearance (n = 7 animals, $p < 0.05$ *vs.* Veh, Fig. 6g) and improved neurobehavioral deficits (n = 6 animals, $p < 0.05$ *vs.* Veh, Fig. 6h). Of note, the number of MMΦ in the perihematomal region was also not notably changed after 4-OI administration (n = 4–7 animals, $p > 0.05$ *vs.* Veh, Supplemental Fig. S5h and i). In contrast, mice intracerebroventricularly injected with *Nrf2* siRNA, Nrf2 inhibitor ML385, or CD36 neutralizing antibodies exhibited increased hematoma volume (n = 9 or 10 animals, $p < 0.05$ 4-OI+si*Nrf2* *vs.* 4-OI+si*Ctrl*, or 4-OI+ML385+IgA, 4-OI+Veh+Ab-CD36 *vs.* 4-OI+Veh+IgA, Fig. 6i and k), and exacerbated neurobehavior dysfunction after ICH (n = 10 animals, $p < 0.05$ 4-OI+si*Nrf2* *vs.* 4-OI+si*Ctrl*, or 4-OI+ML385+IgA, 4-OI+Veh+Ab-CD36 *vs.* 4-OI+Veh+IgA, Fig. 6j and l). These results indicate that Irg1/itaconate axis enhances erythrophagocytosis of MMΦ by regulating Nrf2/CD36 axis after ICH *in vivo*.

Irg1/itaconate axis enhances macrophage phagocytosis of *S. aureus* and improves prognosis after acute peritonitis

Macrophages constitute the first line of defense against invading pathogens.[64] *Staphylococcus aureus* (*S. aureus*) is an opportunistic pathogen that is a leading cause of hospital-acquired, healthcare-associated, and community-acquired infections.[65,66] To explore the role of Irg1/itaconate axis in *S. aureus* clearance by macrophages, we incubated small amounts of *S. aureus* with RAW264.7 cells for either 6 or 12 h *in vitro*. Itaconate and 4-OI both decreased extracellular *S. aureus* in medium, indicating that Irg1/itaconate axis promoted macrophages to engulf *S. aureus* (n = 3, Supplemental Fig. S6a). Surprisingly, there were also fewer intracellular *S. aureus* in cells treated with itaconate and 4-OI, indicating that Irg1/itaconate axis also promoted macrophages to kill *S. aureus* (n = 3, Supplemental Fig. S6a). Meanwhile, we used a classical method to assess the bactericidal properties of macrophages. The results also showed that itaconate and 4-OI both decreased intracellular *S. aureus* in cells (n = 3, Supplemental Fig. S6b). These results indicate that Irg1/itaconate axis not only promotes macrophage phagocytosis of *S. aureus* but also the killing of *S. aureus in vitro*.

To investigate the effects of Irg1/itaconate axis on *S. aureus* phagocytosis *in vivo*, *S. aureus* was intraperitoneally injected into mice to establish the acute peritonitis mouse model (Fig. 7a). Peritoneal fluid (PF) was collected, and peritoneal macrophages (PMs) were isolated from *Irg1* cKO and control mice at different time points. PMs from *Irg1* cKO mice engulfed fewer *S. aureus* (n = 80 PMs from 8 animals, $p < 0.001$ *vs.* *Irg1* flox, Fig. 7b and Supplemental Fig. S6c–e). Consistent with this, the *Irg1* cKO mice had a significantly increased number of extracellular *S. aureus* in PF (n = 5 animals, $p < 0.05$ *vs.* *Irg1* flox, Fig. 7c). Bacterial infection induces behavioral alterations.[67] On 3 and 5 d post-infection, *Irg1* cKO mice exhibited decreased travel distance and average speed following *S. aureus* infection assessed with open field tests (n = 9 animals, $p < 0.05$ *vs.* *Irg1* flox, Fig. 7d and Supplemental Fig. S6f). Of note, the lack of *Irg1* in macrophages didn't induce changes in anxiety-like behaviors or body weight loss (n = 8 or 9 animals, $p > 0.05$ *vs.* *Irg1* flox, Supplemental Fig. S6g and h).

Moreover, neutrophils are important phagocytes post-bacterial infection,[68] and we also observed plenty of bacteria-engulfing neutrophils in PF, although there was no difference in the number of *S. aureus* engulfed by neutrophils between *Irg1* cKO and control mice (n = 273–286 peritoneal neutrophils from 6 animals, $p > 0.05$ *vs.* *Irg1* flox, Supplemental Fig. S6i). Furthermore, we fed mice with PLX5622 to deplete macrophages (n = 3 animals, $p < 0.05$ *vs.* AIN-76A, Supplemental Fig. S6j and k)[69,70] or injected Ly6G neutralizing antibodies to deplete neutrophils (n = 10 animals, $p < 0.001$ *vs.* anti-IgG2a, Supplemental Fig. S6l–n).[71,72] 4-OI failed to alter the extracellular bacteria load in the macrophage-depletion mice (n = 5 animals, $p > 0.05$ PLX5622+4-OI *vs.* PLX5622+Veh, Fig. 7e and f), but still effectively exhibited bacteria clearance acceleration in the neutrophil-depletion mice (n = 5 animals, $p < 0.001$ anti-Ly6G+4-OI *vs.* anti-Ly6G+Veh, Fig. 7g and h), strongly suggesting that macrophages are the main effector cells of Irg1/itaconate axis-enhanced bacterial clearance.

Discussion

Itaconate is an important intermediate metabolite in the tricarboxylic acid cycle. Irg1 is the enzyme catalyzing the decarboxylation of *cis*-aconitate to itaconate in the mitochondria.[12,73] Itaconate plays a general role in

treated as indicated and incubated with PKH26-labeled RBCs. Immunofluorescence staining was performed. n = 4, $^{*}p < 0.05$, $^{***}p < 0.001$ *vs.* Hemin+Veh+IgA; $^{\#\#\#}p < 0.001$ *vs.* Hemin+4-OI+IgA. (**i**) The WT BMDMs were treated as indicated and incubated with pH-sensitive latex beads. n = 4, $^{***}p < 0.001$ *vs.* Hemin+Veh+IgA; $^{\#\#\#}p < 0.001$ *vs.* Hemin+4-OI+IgA. Data are presented as mean ± SD. (**b**, **d**, **e**, and **g**) Two-way ANOVA followed Tukey's or Sidak's multiple comparisons test. (**h** and **i**) One-way ANOVA followed Tukey's multiple comparisons test.

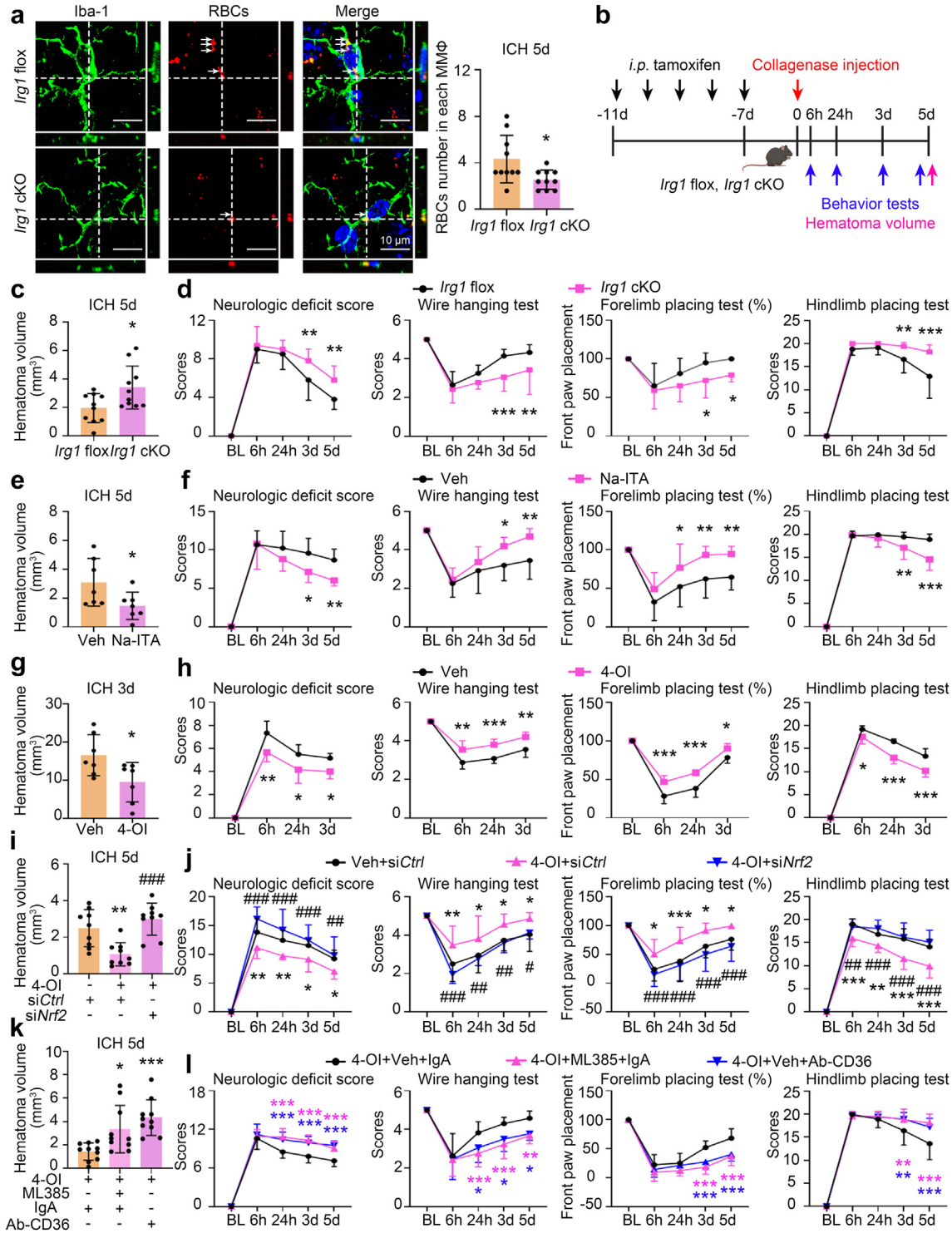

Fig. 6: **Irg1/itaconate axis promotes hematoma clearance and improves acute outcomes after ICH *in vivo*.** (**a**) Six-to-eight-week-old male *Irg1* cKO mice and littermates (*Irg1* flox) underwent injection with PKH26-stained WT RBCs. Brain sections were immunostained with Iba-1 antibodies at 5 d post-injury. White arrows indicate RBCs-engulfing microglia/macrophage. n = 5 animals. Fields calculated for evaluating RBCs number: *Irg1* flox n = 10, *Irg1* cKO n = 10. **p* < 0.05 *vs.* *Irg1* flox. Scale bar = 10 μm. (**b–d**) *Irg1* cKO and *Irg1* flox mice underwent collagenase injection. Schematic experimental procedure (b), hematoma volume (c, n = 10 animals), and behaviors (d, n = 10 animals) are

inhibiting bacterial infections,[18,19,63,74] intracellular viral replication,[20,21] and macrophage inflammation.[13,15,16,22,75] However, whether itaconate controls macrophage phagocytosis and its underlying mechanisms remain unclear. Here, we demonstrated that both itaconate addition and *Irg1* overexpression enhanced macrophage engulfing multiple substrates: live *S. aureus* (the gram-positive bacterium), red blood cells, and dying neuroblastoma cells. Notably, deficiency of *Irg1*-attenuated phagocytosis was effectively rescued by the administration of itaconate or its derivate 4-OI. These data suggest that Irg1/itaconate axis plays an important role in the regulation of macrophage phagocytosis, a function with potential applications in the treatment of multiple diseases. Interestingly, a recent report also revealed that itaconate promoted phagocytosis of *E. coli* (the gram-negative bacterium) by bone marrow-derived macrophages (BMDMs) *in vitro*,[76] suggesting that Irg1/itaconate axis promoted phagocytosis don't have substrate selectivity.

Phagocytosis is a multi-step cellular process involving target cell recognition, cellular engulfment, and lysosomal digestion, and is regulated by receptor–ligand interactions between the target cell and the phagocytes.[77] Macrophages clear pathogens, dead/dying cells, myelin debris, and cell fragments to maintain tissue homeostasis.[78] Scavenger receptors play important roles in regulating macrophage phagocytosis.[79] CD36 is one of the most well-characterized scavenger receptors that regulates macrophage phagocytosis by binding to modified lipids, erythrocytes or apoptotic cells.[80] Cells lacking phagocytic abilities acquire phagocytic functions following transfection with CD36.[81] In preclinical studies, CD36 affects the clearance and uptake of hematoma,[8] myelin debris,[82] oxidized low-density lipoprotein,[83] bacteria,[29] and apoptotic cells[28] in MMΦ. In clinic, CD36-deficient patients have markedly larger hematoma volumes and aggravated neurological deficits in ICH.[84] In our study, we found that the gene encoding CD36 was an overlapped phagocytosis-related gene from ChIP-seq and RNA-seq analyses, and was a major effector of Irg1/itaconate/Keap1/Nrf2-promoted phagocytosis *in vivo* and *in vitro*. Interestingly, although PPARγ is the most-studied transcription factor of *Cd36*,[85] and PPARγ agonists promote macrophage phagocytosis by upregulating CD36 expression,[86–88] we found that treating macrophages with PPARγ inhibitor T0070907 neither affected 4-OI-enhanced CD36 protein level nor -promoted phagocytosis, which indicate that Irg1/itaconate axis regulated macrophage phagocytosis is not through the well-established PPARγ signaling pathway.

Keap1/Nrf2 system forms the major node of cellular and organismal defense against oxidative and electrophilic stresses of both exogenous and endogenous origins.[89] Itaconate has electrophilic properties and directly alkylates cysteine residue on the Keap1 to promote Nrf2 nuclear translocation, activating anti-inflammatory and anti-oxidative genes expression.[13] In our study, we also found that 4-OI upregulated Nrf2-dependent anti-oxidative stress and redox pathways, and anti-inflammatory response, which was consistent with the previously discovered effects of itaconate.[13,53–55,63] Furthermore, we uncovered that itaconate activated Nrf2 to transcribe *Cd36* and then enhanced phagocytosis. Indeed, the direct transcription of *Cd36* by Nrf2 is consistent with previous findings generated by our own lab and others.[42,82,90] We next mutated two potential itaconation sites on Keap1 (cysteine 151 and 288) to explore the molecular mechanism of Irg1/itaconate axis-enhanced phagocytosis. Itaconate covalent modifies the cysteine 151 (C151) on Keap1 to promote the anti-inflammation and anti-oxidative effects of Nrf2,[13,53–55] and cysteine 288 (C288) on Keap1 was identified as a potential itaconation site in a high throughput screening study and hasn't been well studied.[52] Nevertheless, in our study, C151 was still the most important itaconated residue on Keap1, which led to Nrf2-dependent phagocytosis, but not C288. Consistent with our results, the central linker domain in which C288 is located at Keap1 is required for cytoplasmic sequestration of Nrf2,[91] but the mutation of cysteine residues in the linker domain

shown. *$p < 0.05$, **$p < 0.01$, ***$p < 0.001$ *vs.* *Irg1* flox. (**e** and **f**) *Irg1* cKO mice underwent collagenase injection followed by intracerebroventricular injection of 10 mM Na-ITA (in PBS) or vehicle control (PBS) immediately after ICH onset. The hematoma volume (e, n = 7 animals) and neurobehaviors (f, n = 9 animals) are shown. *$p < 0.05$, **$p < 0.01$, ***$p < 0.001$ *vs.* Veh. (**g** and **h**) WT mice underwent collagenase injection followed by intraperitoneal injection of 100 mg/kg 4-OI or vehicle immediately after ICH onset. The hematoma volume (g, n = 7 animals) and neurobehaviors (h, n = 6 animals) are shown. (**i** and **j**) *Nrf2* siRNA or control siRNA (20 pmol/mouse) was intracerebroventricularly injected at 24 h before ICH, and then 100 mg/kg 4-OI or vehicle was intraperitoneally injected immediately after ICH onset. The hematoma volume (i, n = 9 animals) and neurobehaviors (j, n = 10 animals) are shown. *$p < 0.05$, **$p < 0.01$, ***$p < 0.001$ *vs.* Veh+si*Ctrl*; #$p < 0.05$, ##$p < 0.01$, ###$p < 0.001$ *vs.* 4-OI+si*Ctrl*. (**k** and **l**) WT mice underwent collagenase injection followed by intracerebroventricular injection of 50 μM Nrf2 inhibitor ML385, Anti-CD36 antibody [JC63.1] (1:50), IgA-Isotype Control (1:50) or vehicle immediately after ICH onset. Then 4-OI was injected intraperitoneally at 2 h post-injury. The hematoma volume (k, n = 10 animals) and neurobehaviors (l, n = 10 animals) are shown. *$p < 0.05$, **$p < 0.01$, ***$p < 0.001$ *vs.* 4-OI+Veh+IgA. Data are presented as mean ± SD. (**a**, **c**, **e**, and **g**) Two-tailed Student's *t*-test followed by Welch's correction. (**d**, **f**, and **h**) Two-way ANOVA followed Sidak's multiple comparisons test. (**i**) One-way ANOVA followed Tukey's multiple comparisons test. (**j** and **l**) Two-way ANOVA followed Tukey's multiple comparisons test. (**k**) One-way ANOVA followed Dunnett's multiple comparisons test.

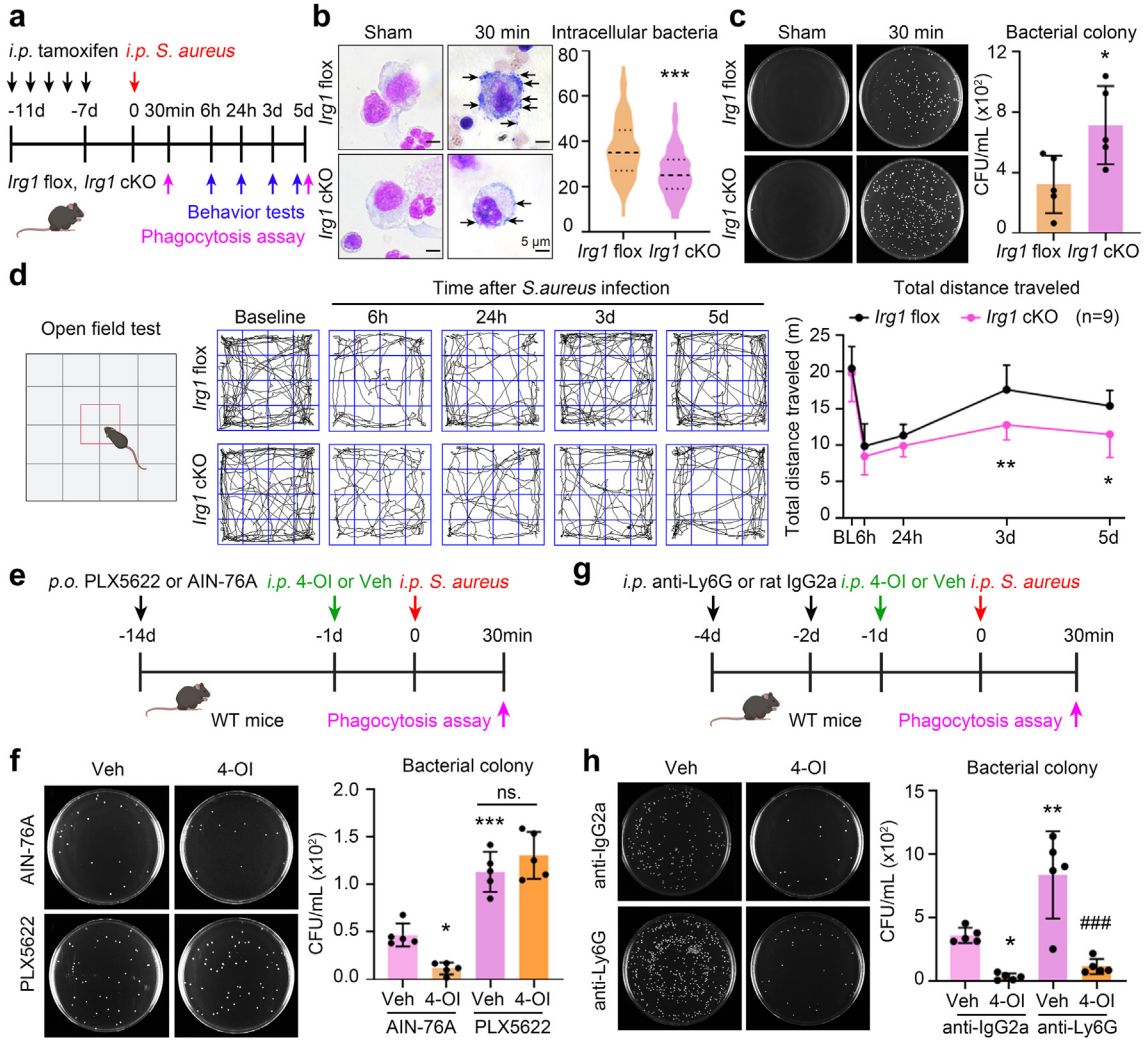

Fig. 7: **Irg1/itaconate axis enhances macrophage phagocytosis of *S. aureus* and improves prognosis after acute peritonitis *in vivo*.** (**a–d**) Male *Irg1* cKO and *Irg1* flox mice were injected with *S. aureus* (*i.p.*). (a) Schematic procedure is shown. (b) Peritoneal macrophages were stained by Wright-Giemsa staining at 30 min after *S. aureus* infection. Black arrows indicate macrophage-engulfed *S. aureus*. n = 8 animals. Peritoneal macrophages calculated for evaluating intracellular bacteria: *Irg1* flox n = 80, *Irg1* cKO n = 80. ***$p < 0.001$ *vs. Irg1* flox, Scale bar = 5 μm. (c) The extracellular *S. aureus* in peritoneal fluids was cultured on the LB agar plates at 30 min after *S. aureus* infection. n = 5 animals. *$p < 0.05$ *vs. Irg1* flox. (d) Motor function was examined after peritonitis by open field test. n = 9 animals. *$p < 0.05$, **$p < 0.01$ *vs. Irg1* flox. (**e** and **f**) MMΦ were pharmacologically depleted with the PLX5622 chow for 14 d. (e) Schematic procedure. (f) The extracellular *S. aureus* in peritoneal fluids was cultured on the LB agar plates at 30 min after *S. aureus* infection. n = 5 animal. *$p < 0.05$, ***$p < 0.001$ *vs.* AIN-76A+Veh; ns., not significant *vs.* PLX5622+Veh. (**g** and **h**) Neutrophils were depleted by intraperitoneal injection of 100 μg Ly6G neutralizing antibodies for 4 d. (g) Schematic procedure. (h) The extracellular *S. aureus* in peritoneal fluids was cultured on the LB agar plates at 30 min after *S. aureus* infection. n = 5 animals. *$p < 0.05$, **$p < 0.01$ *vs.* anti-IgG2a+Veh; ###$p < 0.001$ *vs.* anti-Ly6G+Veh. Data are presented as mean ± SD. (**b** and **c**) Two-tailed Student's *t*-test followed by Welch's correction. (**d**) Two-way ANOVA followed Sidak's multiple comparisons test. (**f** and **h**) One-way ANOVA followed Tukey's multiple comparisons test.

does not perturb the ability of Keap1 to associate with Nrf2,[91] suggesting that C288 is required for Keap1-mediated repression of Nrf2 under basal conditions and Keap1-dependent ubiquitination of Nrf2, while C151 is required for induced escape by Nrf2 from Keap1-mediated repression and Keap1-dependent itaconation of Nrf2.

To confirm the therapeutic effects of Irg1/itaconate axis *in vivo*, we established two mouse models: a collagenase-induced ICH model and an *S. aureus*-injected acute peritonitis model. In the ICH model, we and others, have previously shown activation of microglia and macrophages in the hemorrhagic brain.[8,92] Both populations highly express proinflammatory transcripts

and contribute to acute disability after ICH, and they both gradually switch toward reparative phenotypes to aid in ICH brain repair 3–10 days post-hemorrhage.[8,59,93] In our study, conditional knockout of *Irg1* in MMΦ mice exhibited impaired erythrophagocytosis, delayed hematoma clearance, and aggravated neurobehavior dysfunction in the subacute phase of ICH, while intraperitoneal injection of 4-OI improved outcomes of ICH mice by enhancing hematoma resolution. These data indicate that Irg1/itaconate axis improves ICH prognosis by promoting erythrophagocytosis of macrophages *in vivo*. We further demonstrated that Irg1/itaconate axis in MMΦ mainly affected their engulfing ability and the subsequent prognosis in ICH mice *via* Nrf2/CD36 axis using *Nrf2* silencing, pharmacological inhibitors of Nrf2 and CD36 neutralizing antibodies *in vivo*.

Macrophages are at the crossroads of innate and adaptive immune responses and play an essential role in the control of bacterial infections.[94] A recent report revealed that itaconate promoted macrophages to engulf *E. coli in vitro*.[76] In our study, Irg1/itaconate not only promoted the killing, but also the phagocytosis of *S. aureus in vitro*. In addition, mice with conditional knockout of *Irg1* in macrophages also showed phagocytosis defects to live *S. aureus* after peritonitis infection, thus affecting motor function during infection. However, intraperitoneal injection of 4-OI improved peritoneal macrophages to engulf live *S. aureus*. These results suggest that Irg1/itaconate axis promotes the clearance and killing of live bacteria during infection *in vitro* and *in vivo*. To identify the target cells of bacterial clearance at 30 min after *S. aureus* infection caused by intraperitoneal injection of 4-OI, we demonstrated that macrophages, but not neutrophils, were the main effector cells of Irg1/itaconate axis-enhanced bacterial clearance by depleting macrophages or neutrophils. However, a recent report shows that Irg1 is selectively expressed in neutrophils at 24 h after *S. aureus*-induced pneumonia, and itaconate production impairs neutrophil survival and bacterial killing function.[95] Therefore, the role of Irg1/itaconate axis in neutrophils in a long-term can be further explored in peritonitis in the future.

Our study has some limitations. We only focused on the acute outcomes of ICH and peritonitis, and a long-term study is necessary to be conducted in the future. In addition, administration of 4-OI, si*Nrf2*, ML385, and CD36 neutralizing antibodies was not specific for macrophages *in vivo*, so the clearance of hematoma and *S. aureus* may be synergistic effects of macrophages and other cells. Thus, the development of lipid nanoparticles designed to deliver drugs precisely is a promising therapeutic strategy.

Overall, we found that in different sources of macrophages (mouse bone marrow-derived macrophages, primary microglia, and peritoneal macrophages), different disease models (ICH and peritonitis), Irg1/itaconate axis has a consistent role in promoting macrophage phagocytosis and is regulated by a common Keap1/Nrf2/CD36 molecular mechanism. These findings fill a gap in knowledge regarding the role of itaconate in macrophage phagocytosis, and also provide a vital foundation to develop macrophage-based cell therapy or itaconate-based therapy for treating phagocytosis-related diseases.

Contributors

Conceptualization: ZL, FY, QL Data curation: ZL, LS, DS, LW, FY, QL Formal analysis: ZL, XZ, XW, FY, QL Funding acquisition: QL, FY Investigation: ZL, ZS, LH, LS, YT, WY, FY, QL Methodology: ZL, JA, FY, QL Project administration: JZ, YW, YL, CZ, PW, JA, FY, QL Resources: ZL, ZS, LH, ZX, DS, WW, TL, BZ, FY, QL Software: ZL, WW, DS, CZ, JA, NZ, FY, QL Supervision: FY, QL Validation: ZL, ZS, LS, ZX, DS, FY, QL Visualization: ZL, LW, FY, QL Writing—original draft: ZL, FY, QL Writing—review & editing: ZL, FY, QL.

Data sharing statement

The data that support these findings of the study are available upon request from the corresponding authors.

Declaration of interests

The authors declare no competing interests.

Acknowledgements

We would like to thank Dr. Xiaoling Hu (Capital Medical University, Beijing, China) for providing EGFP transgenic mice for the study. We thank for suggestions from Dr. Xi Wang (Beijing Ditan Hospital, Capital Medical University) and Dr. Guoli Li (Beijing Ditan Hospital, Capital Medical University). This work was supported by the National Natural Science Foundation of China (32070735 and 82371321 to Q. Li, 82271240 to F. Yang) and the Beijing Natural Science Foundation Program and Scientific Research Key Program of Beijing Municipal Commission of Education (KZ202010025033 to Q. Li).

Appendix A. Supplementary data

Supplementary data related to this article can be found at https://doi.org/10.1016/j.ebiom.2024.104993.

References

1 Morrissey MA, Kern N, Vale RD. CD47 ligation repositions the inhibitory receptor SIRPA to suppress integrin activation and phagocytosis. *Immunity*. 2020;53(2):290–302.e6.
2 Gordon S. Phagocytosis: an immunobiologic process. *Immunity*. 2016;44(3):463–475.
3 Erwig LP, Gow NA. Interactions of fungal pathogens with phagocytes. *Nat Rev Microbiol*. 2016;14(3):163–176.
4 Germic N, Frangez Z, Yousefi S, Simon HU. Regulation of the innate immune system by autophagy: monocytes, macrophages, dendritic cells and antigen presentation. *Cell Death Differ*. 2019;26(4):715–727.
5 Hodge S, Hodge G, Scicchitano R, Reynolds PN, Holmes M. Alveolar macrophages from subjects with chronic obstructive pulmonary disease are deficient in their ability to phagocytose apoptotic airway epithelial cells. *Immunol Cell Biol*. 2003;81(4):289–296.
6 Yurdagul A Jr, Subramanian M, Wang X, et al. Macrophage metabolism of apoptotic cell-derived arginine promotes continual efferocytosis and resolution of injury. *Cell Metab*. 2020;31(3):518–533.e10.
7 Hansen DV, Hanson JE, Sheng M. Microglia in Alzheimer's disease. *J Cell Biol*. 2018;217(2):459–472.
8 Li Q, Lan X, Han X, et al. Microglia-derived interleukin-10 accelerates post-intracerebral hemorrhage hematoma clearance by regulating CD36. *Brain Behav Immun*. 2021;94:437–457.
9 Lan X, Han X, Li Q, Yang QW, Wang J. Modulators of microglial activation and polarization after intracerebral haemorrhage. *Nat Rev Neurol*. 2017;13(7):420–433.

10 Advani R, Flinn I, Popplewell L, et al. CD47 blockade by Hu5F9-G4 and rituximab in non-Hodgkin's lymphoma. *N Engl J Med*. 2018;379(18):1711–1721.
11 Joffe AM, Bakalar MH, Fletcher DA. Macrophage phagocytosis assay with reconstituted target particles. *Nat Protoc*. 2020;15(7):2230–2246.
12 Strelko CL, Lu W, Dufort FJ, et al. Itaconic acid is a mammalian metabolite induced during macrophage activation. *J Am Chem Soc*. 2011;133(41):16386–16389.
13 Mills EL, Ryan DG, Prag HA, et al. Itaconate is an anti-inflammatory metabolite that activates Nrf2 via alkylation of KEAP1. *Nature*. 2018;556(7699):113–117.
14 Qin W, Qin K, Zhang Y, et al. S-glycosylation-based cysteine profiling reveals regulation of glycolysis by itaconate. *Nat Chem Biol*. 2019;15(10):983–991.
15 Liao ST, Han C, Xu DQ, Fu XW, Wang JS, Kong LY. 4-Octyl itaconate inhibits aerobic glycolysis by targeting GAPDH to exert anti-inflammatory effects. *Nat Commun*. 2019;10(1):5091.
16 Hooftman A, Angiari S, Hester S, et al. The immunomodulatory metabolite itaconate modifies NLRP3 and inhibits inflammasome activation. *Cell Metab*. 2020;32(3):468–478.e7.
17 Runtsch MC, Angiari S, Hooftman A, et al. Itaconate and itaconate derivatives target JAK1 to suppress alternative activation of macrophages. *Cell Metab*. 2022;34(3):487–501.e8.
18 McFadden BA, Purohit S. Itaconate, an isocitrate lyase-directed inhibitor in Pseudomonas indigofera. *J Bacteriol*. 1977;131(1):136–144.
19 Ruetz M, Campanello GC, Purchal M, et al. Itaconyl-CoA forms a stable biradical in methylmalonyl-CoA mutase and derails its activity and repair. *Science*. 2019;366(6465):589–593.
20 Daniels BP, Kofman SB, Smith JR, et al. The nucleotide sensor ZBP1 and kinase RIPK3 induce the enzyme IRG1 to promote an antiviral metabolic state in neurons. *Immunity*. 2019;50(1):64–76.e4.
21 Olagnier D, Farahani E, Thyrsted J, et al. SARS-CoV2-mediated suppression of NRF2-signaling reveals potent antiviral and anti-inflammatory activity of 4-octyl-itaconate and dimethyl fumarate. *Nat Commun*. 2020;11(1):4938.
22 Lampropoulou V, Sergushichev A, Bambouskova M, et al. Itaconate links inhibition of succinate dehydrogenase with macrophage metabolic remodeling and regulation of inflammation. *Cell Metab*. 2016;24(1):158–166.
23 Chen LL, Morcelle C, Cheng ZL, et al. Itaconate inhibits TET DNA dioxygenases to dampen inflammatory responses. *Nat Cell Biol*. 2022;24(3):353–363.
24 Ogger PP, Albers GJ, Hewitt RJ, et al. Itaconate controls the severity of pulmonary fibrosis. *Sci Immunol*. 2020;5(52):eabc1884.
25 Stuart LM, Ezekowitz RA. Phagocytosis and comparative innate immunity: learning on the fly. *Nat Rev Immunol*. 2008;8(2):131–141.
26 Chen S, Lai SWT, Brown CE, Feng M. Harnessing and enhancing macrophage phagocytosis for cancer therapy. *Front Immunol*. 2021;12:635173.
27 Silverstein RL, Febbraio M. CD36, a scavenger receptor involved in immunity, metabolism, angiogenesis, and behavior. *Sci Signal*. 2009;2(72):re3.
28 Greenberg ME, Sun M, Zhang R, Febbraio M, Silverstein R, Hazen SL. Oxidized phosphatidylserine-CD36 interactions play an essential role in macrophage-dependent phagocytosis of apoptotic cells. *J Exp Med*. 2006;203(12):2613–2625.
29 Stuart LM, Deng J, Silver JM, et al. Response to Staphylococcus aureus requires CD36-mediated phagocytosis triggered by the COOH-terminal cytoplasmic domain. *J Cell Biol*. 2005;170(3):477–485.
30 Means TK, Mylonakis E, Tampakakis E, et al. Evolutionarily conserved recognition and innate immunity to fungal pathogens by the scavenger receptors SCARF1 and CD36. *J Exp Med*. 2009;206(3):637–653.
31 Kumar V, Everingham S, Hall C, Greer PA, Craig AW. Calpains promote neutrophil recruitment and bacterial clearance in an acute bacterial peritonitis model. *Eur J Immunol*. 2014;44(3):831–841.
32 Pan RY, Ma J, Kong XX, et al. Sodium rutin ameliorates Alzheimer's disease-like pathology by enhancing microglial amyloid-beta clearance. *Sci Adv*. 2019;5(2):eaau6328.
33 Roquilly A, Jacqueline C, Davieau M, et al. Alveolar macrophages are epigenetically altered after inflammation, leading to long-term lung immunoparalysis. *Nat Immunol*. 2020;21(6):636–648.
34 Fernando SM, Qureshi D, Talarico R, et al. Intracerebral hemorrhage incidence, mortality, and association with oral anticoagulation use: a population study. *Stroke*. 2021;52(5):1673–1681.
35 Krishnamurthi RV, Feigin VL, Forouzanfar MH, et al. Global and regional burden of first-ever ischaemic and haemorrhagic stroke during 1990-2010: findings from the Global Burden of Disease Study 2010. *Lancet Glob Health*. 2013;1(5):e259–e281.
36 Broderick JP, Brott TG, Duldner JE, Tomsick T, Huster G. Volume of intracerebral hemorrhage. A powerful and easy-to-use predictor of 30-day mortality. *Stroke*. 1993;24(7):987–993.
37 Gonzales NR, Shah J, Sangha N, et al. Design of a prospective, dose-escalation study evaluating the Safety of Pioglitazone for hematoma Resolution in Intracerebral Hemorrhage (SHRINC). *Int J Stroke*. 2013;8(5):388–396.
38 von Graevenitz A, Amsterdam D. Microbiological aspects of peritonitis associated with continuous ambulatory peritoneal dialysis. *Clin Microbiol Rev*. 1992;5(1):36–48.
39 Okabe M, Ikawa M, Kominami K, Nakanishi T, Nishimune Y. 'Green mice' as a source of ubiquitous green cells. *FEBS Lett*. 1997;407(3):313–319.
40 Park SY, Jung MY, Kim HJ, et al. Rapid cell corpse clearance by stabilin-2, a membrane phosphatidylserine receptor. *Cell Death Differ*. 2008;15(1):192–201.
41 Subramanian S, Busch CJ, Molawi K, et al. Long-term culture-expanded alveolar macrophages restore their full epigenetic identity after transfer in vivo. *Nat Immunol*. 2022;23(3):458–468.
42 Liu J, Shen D, Wei C, et al. Inhibition of the LRRC8A channel promotes microglia/macrophage phagocytosis and improves outcomes after intracerebral hemorrhagic stroke. *iScience*. 2022;25(12):105527.
43 Xiao Z, Shen D, Lan T, et al. Reduction of lactoferrin aggravates neuronal ferroptosis after intracerebral hemorrhagic stroke in hyperglycemic mice. *Redox Biol*. 2022;50:102256.
44 Vega-Perez A, Villarrubia LH, Godio C, et al. Resident macrophage-dependent immune cell scaffolds drive anti-bacterial defense in the peritoneal cavity. *Immunity*. 2021;54(11):2578–2594.e5.
45 Nobs SP, Kolodziejczyk AA, Adler L, et al. Lung dendritic-cell metabolism underlies susceptibility to viral infection in diabetes. *Nature*. 2023;624:645–652.
46 Li Q, Han X, Lan X, et al. Inhibition of neuronal ferroptosis protects hemorrhagic brain. *JCI Insight*. 2017;2(7):e90777.
47 Wu H, Wu T, Xu X, Wang J, Wang J. Iron toxicity in mice with collagenase-induced intracerebral hemorrhage. *J Cereb Blood Flow Metab*. 2011;31(5):1243–1250.
48 Riquelme SA, Liimatta K, Wong Fok Lung T, et al. Pseudomonas aeruginosa utilizes host-derived itaconate to redirect its metabolism to promote biofilm formation. *Cell Metab*. 2020;31(6):1091–1106.e6.
49 Luo B, Gan W, Liu Z, et al. Erythropoeitin signaling in macrophages promotes dying cell clearance and immune tolerance. *Immunity*. 2016;44(2):287–302.
50 Bewley MA, Budd RC, Ryan E, et al. Opsonic phagocytosis in chronic obstructive pulmonary disease is enhanced by Nrf2 agonists. *Am J Respir Crit Care Med*. 2018;198(6):739–750.
51 Crisman E, Duarte P, Dauden E, et al. KEAP1-NRF2 protein-protein interaction inhibitors: design, pharmacological properties and therapeutic potential. *Med Res Rev*. 2023;43(1):237–287.
52 Qin W, Zhang Y, Tang H, et al. Chemoproteomic profiling of itaconation by bioorthogonal probes in inflammatory macrophages. *J Am Chem Soc*. 2020;142(25):10894–10898.
53 Song H, Xu T, Feng X, et al. Itaconate prevents abdominal aortic aneurysm formation through inhibiting inflammation via activation of Nrf2. *eBioMedicine*. 2020;57:102832.
54 Liu H, Feng Y, Xu M, Yang J, Wang Z, Di G. Four-octyl itaconate activates Keap1-Nrf2 signaling to protect neuronal cells from hydrogen peroxide. *Cell Commun Signal*. 2018;16(1):81.
55 Tang C, Tan S, Zhang Y, Dong L, Xu Y. Activation of Keap1-Nrf2 signaling by 4-octyl itaconate protects human umbilical vein endothelial cells from high glucose. *Biochem Biophys Res Commun*. 2019;508(3):921–927.
56 Li W, Li Y, Kang J, et al. 4-octyl itaconate as a metabolite derivative inhibits inflammation via alkylation of STING. *Cell Rep*. 2023;42(3):112145.
57 Magid-Bernstein J, Girard R, Polster S, et al. Cerebral hemorrhage: pathophysiology, treatment, and future directions. *Circ Res*. 2022;130(8):1204–1229.
58 Chang CF, Goods BA, Askenase MH, et al. Divergent functions of tissue-resident and blood-derived macrophages in the hemorrhagic brain. *Stroke*. 2021;52(5):1798–1808.

59 Chang CF, Goods BA, Askenase MH, et al. Erythrocyte efferocytosis modulates macrophages towards recovery after intracerebral hemorrhage. *J Clin Invest*. 2018;128(2):607–624.
60 Laird MD, Wakade C, Alleyne CH Jr, Dhandapani KM. Hemin-induced necroptosis involves glutathione depletion in mouse astrocytes. *Free Radic Biol Med*. 2008;45(8):1103–1114.
61 Yan X, He M, Huang H, et al. Endogenous H(2)S targets mitochondria to promote continual phagocytosis of erythrocytes by microglia after intracerebral hemorrhage. *Redox Biol*. 2022;56:102442.
62 Prinz M, Priller J. Microglia and brain macrophages in the molecular age: from origin to neuropsychiatric disease. *Nat Rev Neurosci*. 2014;15(5):300–312.
63 Singh S, Singh PK, Jha A, et al. Integrative metabolomics and transcriptomics identifies itaconate as an adjunct therapy to treat ocular bacterial infection. *Cell Rep Med*. 2021;2(5):100277.
64 Mogensen TH. Pathogen recognition and inflammatory signaling in innate immune defenses. *Clin Microbiol Rev*. 2009;22(2):240–273 [Table of Contents].
65 Kaech C, Elzi L, Sendi P, et al. Course and outcome of Staphylococcus aureus bacteraemia: a retrospective analysis of 308 episodes in a Swiss Tertiary-Care Centre. *Clin Microbiol Infect*. 2006;12(4):345–352.
66 Abdulgader SM, van Rijswijk A, Whitelaw A, Newton-Foot M. The association between pathogen factors and clinical outcomes in patients with Staphylococcus aureus bacteraemia in a tertiary hospital, Cape Town. *Int J Infect Dis*. 2020;91:111–118.
67 Chen Q, Tarr AJ, Liu X, et al. Controlled progressive innate immune stimulation regimen prevents the induction of sickness behavior in the open field test. *J Inflamm Res*. 2013;6:91–98.
68 Appelberg R. Neutrophils and intracellular pathogens: beyond phagocytosis and killing. *Trends Microbiol*. 2007;15(2):87–92.
69 Elmore MR, Najafi AR, Koike MA, et al. Colony-stimulating factor 1 receptor signaling is necessary for microglia viability, unmasking a microglia progenitor cell in the adult brain. *Neuron*. 2014;82(2):380–397.
70 Almonte VM, Uriyanghai U, Egana-Gorrono L, et al. PLX3397, a CSF1 receptor inhibitor, limits allotransplantation-induced vascular remodeling. *Cardiovasc Res*. 2022;118(12):2718–2731.
71 Herz J, Sabellek P, Lane TE, Gunzer M, Hermann DM, Doeppner TR. Role of neutrophils in exacerbation of brain injury after focal cerebral ischemia in hyperlipidemic mice. *Stroke*. 2015;46(10):2916–2925.
72 Loi P, Yuan Q, Torres D, et al. Interferon regulatory factor 3 deficiency leads to interleukin-17-mediated liver ischemia-reperfusion injury. *Hepatology*. 2013;57(1):351–361.
73 Michelucci A, Cordes T, Ghelfi J, et al. Immune-responsive gene 1 protein links metabolism to immunity by catalyzing itaconic acid production. *Proc Natl Acad Sci U S A*. 2013;110(19):7820–7825.
74 Nguyen TV, Alfaro AC, Young T, Green S, Zarate E, Merien F. Itaconic acid inhibits growth of a pathogenic marine Vibrio strain: a metabolomics approach. *Sci Rep*. 2019;9(1):5937.
75 Bambouskova M, Gorvel L, Lampropoulou V, et al. Electrophilic properties of itaconate and derivatives regulate the IkappaBzeta-ATF3 inflammatory axis. *Nature*. 2018;556(7702):501–504.
76 O'Callaghan AA, Dempsey E, Iyer N, Stiegeler S, Mercurio K, Corr SC. Intestinal metabolites influence macrophage phagocytosis and clearance of bacterial infection. *Front Cell Infect Microbiol*. 2021;11:622491.
77 Feng M, Jiang W, Kim BYS, Zhang CC, Fu YX, Weissman IL. Phagocytosis checkpoints as new targets for cancer immunotherapy. *Nat Rev Cancer*. 2019;19(10):568–586.
78 Van Broeckhoven J, Sommer D, Dooley D, Hendrix S, Franssen A. Macrophage phagocytosis after spinal cord injury: when friends become foes. *Brain*. 2021;144(10):2933–2945.
79 Freeman SA, Grinstein S. Phagocytosis: receptors, signal integration, and the cytoskeleton. *Immunol Rev*. 2014;262(1):193–215.
80 Chen Y, Zhang J, Cui W, Silverstein RL. CD36, a signaling receptor and fatty acid transporter that regulates immune cell metabolism and fate. *J Exp Med*. 2022;219(6):e20211314.
81 Ren Y, Silverstein RL, Allen J, Savill J. CD36 gene transfer confers capacity for phagocytosis of cells undergoing apoptosis. *J Exp Med*. 1995;181(5):1857–1862.
82 Grajchen E, Wouters E, van de Haterd B, et al. CD36-mediated uptake of myelin debris by macrophages and microglia reduces neuroinflammation. *J Neuroinflammation*. 2020;17(1):224.
83 Pokhrel S, Gudneppanavar R, Teegala LR, Duah E, Thodeti CK, Paruchuri S. Leukotriene D4 upregulates oxidized low-density lipoprotein receptor 1 and CD36 to enhance oxidized LDL uptake and phagocytosis in macrophages through cysteinyl leukotriene receptor 1. *Front Physiol*. 2021;12:756450.
84 Fang H, Chen J, Lin S, et al. CD36-mediated hematoma absorption following intracerebral hemorrhage: negative regulation by TLR4 signaling. *J Immunol*. 2014;192(12):5984–5992.
85 Tontonoz P, Nagy L, Alvarez JG, Thomazy VA, Evans RM. PPARgamma promotes monocyte/macrophage differentiation and uptake of oxidized LDL. *Cell*. 1998;93(2):241–252.
86 Flores JJ, Klebe D, Rolland WB, Lekic T, Krafft PR, Zhang JH. PPARgamma-induced upregulation of CD36 enhances hematoma resolution and attenuates long-term neurological deficits after germinal matrix hemorrhage in neonatal rats. *Neurobiol Dis*. 2016;87:124–133.
87 Mu Q, Wang L, Hang H, Liu C, Wu G. Rosiglitazone pretreatment influences thrombin-induced phagocytosis by rat microglia via activating PPARgamma and CD36. *Neurosci Lett*. 2017;651:159–164.
88 Wang Y, Chen Q, Tan Q, et al. Simvastatin accelerates hematoma resolution after intracerebral hemorrhage in a PPARgamma-dependent manner. *Neuropharmacology*. 2018;128:244–254.
89 Yamamoto M, Kensler TW, Motohashi H. The KEAP1-NRF2 system: a thiol-based sensor-effector apparatus for maintaining redox homeostasis. *Physiol Rev*. 2018;98(3):1169–1203.
90 Olagnier D, Lavergne RA, Meunier E, et al. Nrf2, a PPARgamma alternative pathway to promote CD36 expression on inflammatory macrophages: implication for malaria. *PLoS Pathog*. 2011;7(9):e1002254.
91 Zhang DD, Hannink M. Distinct cysteine residues in Keap1 are required for Keap1-dependent ubiquitination of Nrf2 and for stabilization of Nrf2 by chemopreventive agents and oxidative stress. *Mol Cell Biol*. 2003;23(22):8137–8151.
92 Chang CF, Massey J, Osherov A, Angenendt da Costa LH, Sansing LH. Bexarotene enhances macrophage erythrophagocytosis and hematoma clearance in experimental intracerebral hemorrhage. *Stroke*. 2020;51(2):612–618.
93 Taylor RA, Chang CF, Goods BA, et al. TGF-beta1 modulates microglial phenotype and promotes recovery after intracerebral hemorrhage. *J Clin Invest*. 2017;127(1):280–292.
94 Hmama Z, Pena-Diaz S, Joseph S, Av-Gay Y. Immunoevasion and immunosuppression of the macrophage by Mycobacterium tuberculosis. *Immunol Rev*. 2015;264(1):220–232.
95 Tomlinson KL, Riquelme SA, Baskota SU, et al. Staphylococcus aureus stimulates neutrophil itaconate production that suppresses the oxidative burst. *Cell Rep*. 2023;42(2):112064.